Epigenic vs. hypogenic speleogenesis governed by H2S/CO2 hydrothermal input and Quaternary icefield dynamics (NE French Pyrenees)

Dimitri Laurent, Christophe Durlet, Guillaume Barré, Patrick Sorriaux, Philippe Audra, Pierre Cartigny, Cédric Carpentier, Guillaume Paris, Pauline Collon, Thomas Rigaudier, et al.

Geomorphology, 387: 107769, 2021
10.1016/j.geomorph.2021.107769

Epigenic vs. hypogenic speleogenesis governed by H_2S/CO_2 hydrothermal input and Quaternary icefield dynamics (NE French Pyrenees)

Dimitri Laurent[a*], Christophe Durlet[b], Guillaume Barré[cd], Patrick Sorriaux[e], Philippe Audra[f], Pierre Cartigny[g], Cédric Carpentier[a], Guillaume Paris[h], Pauline Collon[a], Thomas Rigaudier[h], Jacques Pironon[a], Eric C. Gaucher[c]

[a] *Université de Lorraine, CNRS, CREGU, GeoRessources, F-54000 Nancy, France*
[b] *Biogéosciences, UMR 6282 CNRS, Université Bourgogne Franche-Comté, 21000 Dijon, France*
[c] *TOTAL, Scientific and Technical Center Jean Féger (CSTJF), 64000 Pau, France*
[d] *Université de Pau et Pays de l'Adour, E2S UPPA, CNRS, TOTAL, LFCR, UMR5150, 64000 Pau, France*
[e] *Retired petroleum geoscientist TOTAL, 09400 Bédeilhac, France.*
[f] *Polytech Lab UPR 7498, University Côte d'Azur, Nice, France*
[g] *Université de Paris, Institut de Physique du Globe de Paris, CNRS, 75005 Paris, France*
[h] *Centre de Recherches Pétrographiques et Géochimiques CRPG, CNRS, Vandœuvre-lès-Nancy, France.*

Abstract Hypogenic caves, linked to carbonate rock dissolution due to CO_2- and H_2S-rich ascending deep waters, represent more than 10% of karstic networks worldwide; a proportion that increases as these systems are better constrained. However, interaction between hypogenic and epigenic processes is still poorly understood, especially since the subsequent invasion of surface water often obliterates the morphological and mineral markers of hypogenic activities. The Ariège Valley (French Pyrenean foothills) hosts significant karstic networks epigenically reworked by several episodes of glacier meltwater penetration during the successive coverage of Quaternary icefields. Among these karstic systems, the Vapeur and Ermite caves were probably initiated by a hypogenic component during the Miocene. In particular, multiple-S, Sr, H, C, and O isotopes of thermo-mineral waters and calcite-sulfate speleothems confirm that hydrothermal fluids reached the caves, and subsequently interacted with Quaternary glacial epigenic phases. Deep fluids conveyed CO_2 and H_2S, both produced from the thermochemical reduction of Triassic evaporites at depth. H_2S oxidation and CO_2 hydration in the cave atmosphere, above the water table, created sulfuric and carbonic acids responsible for an intense karstification. Interpretation of isotopic data, together with a geomorphological, mineralogical and textural study of cave minerals, allow us to propose a speleogenetic model in which the respective impact of epigenic and hypogenic processes was driven by base-level changes during successive Quaternary glacial/interglacial epochs: (i) during glacial periods, invasion of glacier meltwater within the karst led to the dilution of the hydrothermal water, and was responsible for an *"epigenic mechanical-dominant"* speleogenesis through water-related abrasion; (ii) interglacial epochs were marked by base-level drops and the establishment of a vadose domain in caves, favoring the widening of karstic conduits through carbonic and sulfuric acid condensation-corrosion during thermal water degassing. This *"hypogenic chemical-dominant"* speleogenesis was active until a new advance of glaciers, and this cycle occurred several times.

Keywords: Hypogene sulfuric and carbonic acid speleogenesis; Multiple sulfur isotopes; Thermal water geochemistry; Pyrenees.

1. Introduction

The understanding of karstic system genesis and evolution is of primary importance as carbonate rocks cover c.a. 15.2% of the planet's dry ice-free land and as 1.18 billion people (16.5% of the global population) live on karst and thus depend on the karst water management strategy (Ford and Williams, 2007; Goldscheider et al., 2020). Among all the identified karstic networks, at least 10% are defined as "hypogenic" (Palmer, 1991; Palmer and Palmer, 2000). Hypogenic processes imply that acidity comes from deep-rooted upward recharge (Plan et al., 2012; Tisato

et al., 2012; Klimchouk et al., 2017; Pérez-Mejías et al., 2019; Klanica et al., 2020), rather than epigenic origin (fully formed by water movement coming from overlying or adjacent recharge surfaces; e.g. Palmer, 1991). Deep fluids involved in hypogenic speleogenesis are commonly rich in CO_2 and/or H_2S, and can derived from various hydrothermal sources such as mantellic, volcanic, metamorphic or buried basinal fluids (Klimchouk et al., 2017 and references therein). Among hypogenic caves, deep-seated karsts can develop at great depth (e.g. Forti and Sanna, 2010), while shallow caves also formed at former water table levels (De Waele et al., 2016; D'Angeli et al., 2019). Attempts to discriminate between hypogenic and epigenic caves are very recent, and mostly developed during the past two decades (e.g. Klimchouk, 2007). Since then, a lot of caves have been revisited and classified as hypogenic. Their distinction remains challenging because of the overprinting of most hypogenic morphologies by subsequent meteoric processes occurring in late stages (e.g. Columbu et al., 2021), frequently after exhumation of carbonate massifs. A common approach considers the description of typical morphologies attributed to epigenic and hypogenic karsts, together with the identification of the fluid nature and regional migration pathways that controlled the timing and loci of the karst (Klimchouk et al., 2017). When considering composition of acidic fluids, four main classes of hypogenic karsts are commonly considered (e.g. Palmer, 1991): (i) carbonic acid speleogenesis derived from deep-seated CO_2-rich fluids associated with *in-situ* hydration of CO_2 to H_2CO_3 (e.g. Piccini, 2000; Ford and Williams, 2007; Sarbu and Lascu 1997; Leél-Őssy, 2017); (ii) Sulfuric Acid Speleogenesis (SAS) linked to the oxidation of deep H_2S to sulfuric acid H_2SO_4 (Egemeier, 1981), at or close to the water table (Audra, 2007; Audra et al., 2007a; De Waele et al., 2016; D'Angeli et al., 2019), intensively dissolving carbonate rocks and precipitating significant amounts of gypsum deposits (e.g. Galdenzi and Maruoka, 2003); (iii) "gypsum karsts" in which a meteoric recharge flowing across deep carbonate aquifers is responsible for *per ascensum* fluid migration into overlying gypsum formations that are dissolved without involving a high content of CO_2 or H_2S (Klimchouk et al., 2017 and references therein); and (iv) coastal mixing caves or flank margin caves formed by the interaction between fresh-water and salt-water which causes a mixing dissolution process, and also produces organic-trapping horizons enhancing the dissolution through the generation of CO_2 (Mylroie, 1988; Palmer, 1991; Mylroie and Mylroie, 2007; Lopez-Martinez et al., 2020).

Our study will only be focused on carbonic and sulfuric acid caves. In most investigations, hypogenic carbonic karstification is identified through the confrontation between specific textures of calcite precipitates (rafts, folia, spar linings, mammillaries, popcorn…; e.g. Audra et al., 2007a; Hill and Polyak, 2010), their carbon and oxygen isotopic composition (Sarbu and Lascu, 1997; Dublyansky and Spötl, 2009; Temovski et al., 2013; Dublyansky et al., 2014; Klimchouk et al., 2014; Klimchouk et al., 2017) and fluid inclusion microthermometry (e.g. Hill, 1987; Dublyansky and Spötl, 2009).

SAS is particularly important as it generates large karstic networks one to two orders of magnitude faster than "classical" epigenic and carbonic acid-derived karsts (De Waele et al., 2016). In addition to hypogenic morphologies similar to carbonic acid speleogenesis, the identification of SAS is mainly based on major sulfur isotopes (^{32}S and ^{34}S) of the gypsum precipitated in replacement of the host carbonate rock (e.g. Hill, 1987; Onac et al., 2011; Temovski et al., 2018), which allow to decipher the action of sulfuric acid from the simple precipitation from sulfate-supersaturated solutions in caves. However, major sulfur isotope ratios do not permit to accurately identify the different natures, variability and mixing of multiple sulfur sources, which can be more accurately constrained using Multiple Sulfur Isotopes (MSI, also studying the ^{33}S; e.g. Farquhar et al., 2007). Yet, MSI remains very rarely used in karst studies (Zerkle et al., 2016).

Cretaceous and Jurassic formations in the South Aquitaine Basin and northern Pyrenean foothills basins (Southwest of France) contain a significant concentration of thermogenic H_2S (Biteau et al., 2006), which could have played a role in SAS for some karstic systems. To document the variability and the extension of hypogenic karstification in the Pyrenean foothill basins, the present work discusses the speleogenesis of two specific caves located in the northeastern Pyrenees: the Vapeur and Ermite caves in the Ariège Valley, both connected to the same thermo-mineral spring. In order to evaluate the possible action of hypogenic processes responsible for the genesis and/or for the geomorphological evolution of these cavities, this study includes several approaches: (i) morphologies of galleries and textures of various speleothems, (ii) mineralogy and geochemistry of speleothems; (iii) various isotopic compositions (sulfur, oxygen, hydrogen, carbon and strontium) of thermo-mineral waters to decipher their origin, together with a comparison with speleothems'

isotopic signatures (calcite and sulfate minerals) to infer a potential link with the hydrothermal activity. We finally propose an integrated genetic model in which the Quaternary hydrogeological evolution of both the Vapeur and Ermite caves is intimately linked to the hydrodynamics and base-level changes during glacial/interglacial periods, that control the relative contribution of both epigenic and hypogenic processes; the latter process being linked to the deep circulation of thermochemical CO_2 and H_2S.

2. Regional context of Ariège Valley caves

2.1. Architecture and stratigraphy of the Tarascon-sur-Ariège basin

The Vapeur and Ermite caves are located on the eastern flank of the Ariège Valley which overlooks the village of Ussat-les-Bains, in the southern part of the Tarascon-sur-Ariège basin (Fig.1a). The two neighboring caves develop within metamorphosed Aptian limestones (Urgonian Facies), with entrances at an altitude of 560 m for the Vapeur Cave and at 550 m for the Ermite Cave (around 80 m above the Ariège River). The Tarascon-sur-Ariège basin constitutes a synclinorium bordered by the Variscan massifs of Aston in the south, St-Barthélémy in the east, Arize in the north, and Trois-Seigneurs in the west (Fig.1a). Above Triassic series, composed of marls and evaporites, the sedimentary pile is formed by a thick series of Jurassic to Cretaceous limestones, dolostones and marls in a stack of asymmetrical anticlines verging to the south (Fig.1b).

In the vicinity of both Vapeur and Ermite caves, at Ussat-les-Bains (see Fig.1a for location), a borehole drilled for geothermal exploration, provides a detailed stratigraphical section of underlying strata (Fig.2): 114 m of glaciofluvial alluvium (blocks, sand and sandy shales) filling the Ariège Valley, 934 m of Cretaceous and Jurassic carbonate formations, 40 m of Keuper gypsum-rich clays, and finally the Paleozoic basement composed of schists beyond 1088 m depth (Antea, 2009). Within the 934 m of Mesozoic carbonate series, the first hundred meters are composed of Neocomian beige/yellow micritic limestones and gravelly carbonates, which downwards pass to homogeneous beige limestones between 209 and 319 m, and finally to the Liassic limestones down to 1048 m, alternating with some thin ophitic layers just before the underlying contact with the Triassic evaporitic series. Not crossed by the borehole, the Aptian sedimentary series, which overlay the Neocomian carbonates, outcrop both on the eastern and western flanks of the Ariège Valley (Fig.1b), easily recognizable by the presence of *Toucasia* rudists in the Urgonian limestones. The studied Vapeur and Ermite caves developed essentially in this Urgonian facies.

All these Mesozoic sediments have been exhumed during the Pyrenean orogeny with the emplacement of an erosional subplanar unconformity during the Neogene, truncating both the Aptian and Albian carbonates and marl series, as well as the surrounding Paleozoic gneissic basement (Calvet, 1996; Monod et al., 2016). After the Pliocene, these massifs have been entrenched by successive Quaternary glacial erosion with icefields entirely covering the sedimentary series (Delmas et al., 2012) which have structured or enhanced the succession of modern N-S valleys.

2.2. Karstic and hydrogeological context of the Ussat-les-Bains massif

Numerous karstic cavities, especially developed in Urgonian limestones, are known in the Ussat-les-Bains massif (e.g. Sorriaux et al., 2016). Among them, the most developed network includes the famous prehistoric Niaux Cave (entrance: altitude of 680 m), Lombrives Cave (entrance: altitude of 600 m) and Sabart Cave (entrance: altitude of 560 m). This karstic network, lying few kilometers northwest from the Vapeur and Ermite caves (Fig.1a), has been subjected to intense geological investigations, including facies description and cosmogenic dating of cave sediments, and U/Th dating of speleothems (Sorriaux, 1982; Bakalowicz et al., 1984; Sorriaux et al., 2016; Sartégou et al., 2020). Most cave systems probably initiated during the Miocene-Pliocene (ages inferred from cosmogenic nuclides at 8.63 ±2.08 Ma of fluvio-karstic sediments; Sartégou et al., 2020), and were then entirely covered and scoured by glaciers during the successive Quaternary glacial periods. Based on U/Th dating of flowstone (Sorriaux, 1982; Bakalowicz et al., 1984; Sorriaux et al., 2016), and cosmogenic nuclides of surrounding moraines (Delmas et al., 2011, 2012), the chronology of karst reactivation by glacial meltwater and sedimentary filling during the different glaciations is well constrained over the last 450 kyr (Sorriaux et al., 2016). These glacial events were particularly active in this area during the Marine Isotopic Stages MIS2, MIS4 and MIS8 (Sorriaux et al., 2016).

In addition to those epigenic events, current active hydrothermal circulations within the Jurassic and Cretaceous limestones of the Ariège Valley implies the

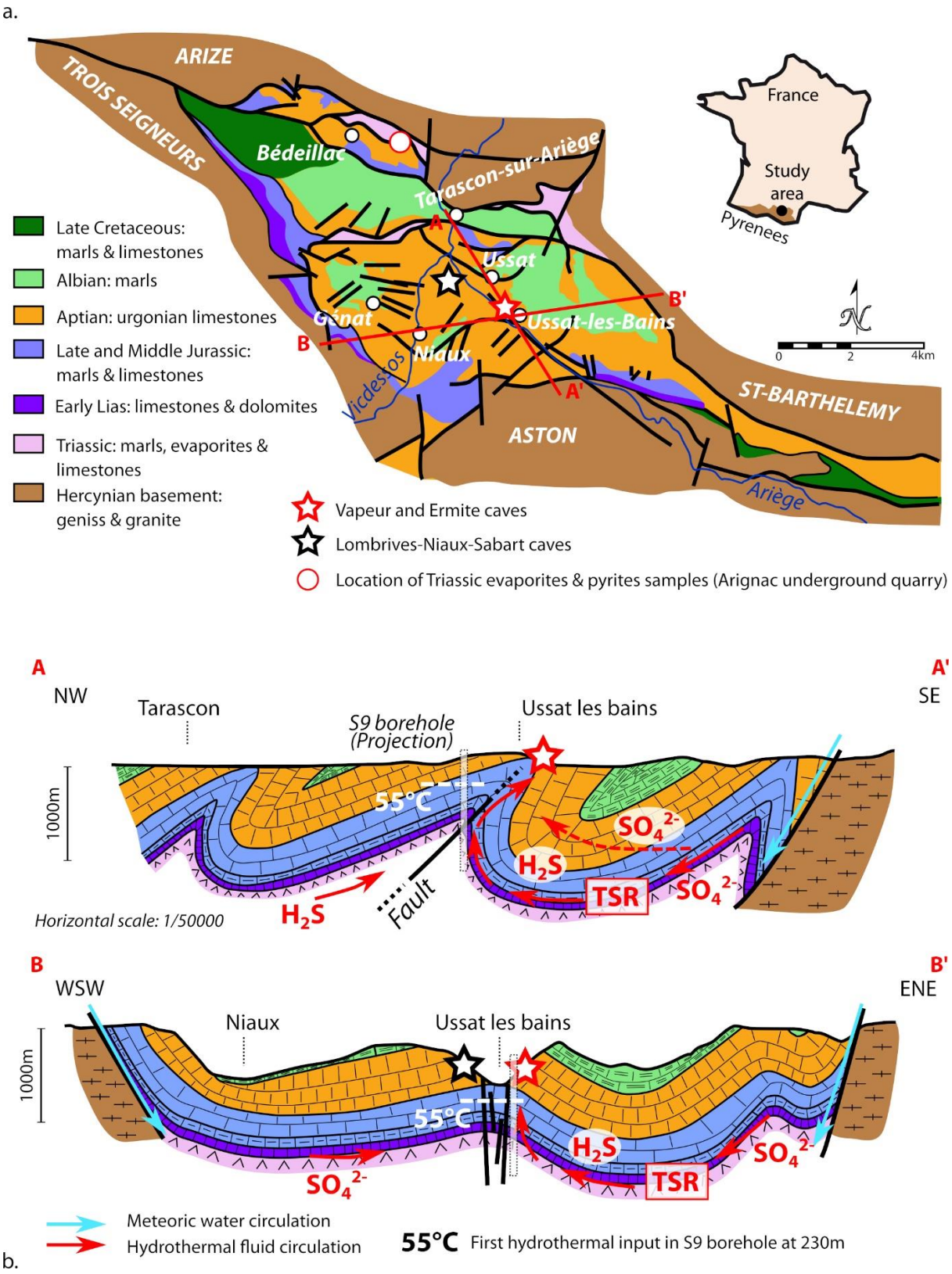

Figure 1: Geological context of the Tarascon-sur-Ariège basin. a. Geological and structural map of the basin. The location of the studied caves (star: Ermite and Vapeur caves), the Niaux-Lombrives-Sabart karstic networks (triangle) and the Arignac underground quarry where Triassic evaporites and pyrites have been sampled (dot) are indicated. b. Fluid flow at the basin scale (arrow) illustrating in NW-SE and WSW-ENE cross sections (respectively lines B-B' and C-C' in Fig.1a; inspired from BRGM, 1983). See explanation of fluid circulation in the discussion part. TSR: Thermochemical Sulfate Reduction. The value 55 °C corresponds to the temperature measurement of the more superficial hydrothermal water input in the S9 borehole at a depth of 230 m (Antea, 2009).

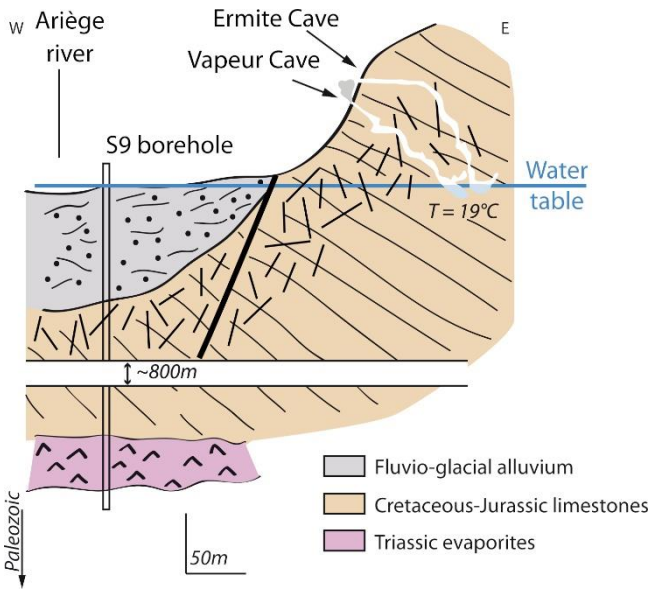

Figure 2: Geological cross section of the Ariège Valley at the location of the Ermite and Vapeur caves, with the indication of current hydrothermal circulations and potential exchanges between the karst and the water table close to the Ariège river (dilution of hydrothermal inputs). The thermal water borehole S9 from which the sedimentological log was defined (Antea, 2009) is reported.

possibility that hypogenic karstification also occurred. Indeed, the valley, near the studied caves, currently hosts a thermal spa implanted close to a thermo-mineral spring in Ussat-les-Bains running across the fluvial sediments and Urgonian limestones. Since 1996, spring-water is captured by the S9 borehole, with pressurized cemented casing, and pumping below the cold-water mixing zone (below 220 m; Antea, 2009). The average temperature of the collected water is 58 °C, and the more superficial hot water inflow in the borehole occurs at a depth of 261 m at a temperature of 55.5 °C (Antea, 2009). Hot waters are trapped in two distinct but hydraulically connected aquifers: the fluvio-glacial alluvium at the bottom of the valley, and the Jurassic-Cretaceous carbonate series where the major part of the large karstic networks is located (Fig.1b and 2). This thermo-mineral water reservoir is laterally delimitated by the gneiss and schist formation of the exhumed Paleozoic basement for a perpendicular and longitudinal extension of 1 km and 6 km with respect to the Ariège Valley axis (Antea, 2009).

3. Data and methods

3.1 Mineralogical characterization

A total of 6 cave sulfate minerals have been characterized on powder using Diffuse Reflectance Infrared Fourier Transform (DRIFT) spectroscopy at the GeoRessources Laboratory (Nancy, France), and X-Ray Diffraction (XRD) at the CRM2 Laboratory (Nancy, France). DRIFT spectra were recorded in the mid-infrared range with a spectral resolution of 2 cm^{-1} using a Fourier transform infrared spectrometer BRUKER IFS 55 and performed on dry samples diluted of 15% by weight in potassium bromide (Kbr). XRD analyses were made using a Bruker D2 phaser with a SSD160 detector and acquisitions collected over the range 2-3 to 70-75° 2θ using a step interval of 0.02° 2θ every 0.6 s. For both methods, obtained spectra were compared to mineral database PDF-2 to identify the exact nature of sulfates.

3.2. *In-situ* gas analyses by the analyzer GA5000

Gas compositions of the cave atmosphere were established using a GA5000 gas analyzer (Geotech[(c)]). This apparatus allows us to analyze the concentration of CH_4 (error of 0.5% of the full scale), CO_2 (error of 0.5%), H_2S (error of 1.5%), O_2 (error of 1%), CO (error of 2%) and H_2 (error of 2.5%).

3.3. Physico-chemical properties of water

Conductivity, pH, temperature and dissolved O_2 of water were measured *in-situ* using a HACH[(c)] HQ30D Kit multimeter with LDO electrodes. Errors are estimated to 0.5% between 1 µS/cm and 200 mS/cm for the conductivity, 0.1°C for the temperature, 0.01 for the pH, and 0.01 mg/l for dissolved O_2.

Chemical analyses of water were carried out in the Total laboratories (Pau, Centre Scientifique et Technique Jean Féger – CSTJF, France) using Ion Chromatography (Cl^-, Br^- and SO_4^{2-}), Inductively Coupled Plasma-Atomic Emission Spectroscopy (Li^+, Br^- and Sr^{2+}), Inductively Coupled Plasma-Mass Spectrometry (Ca^{2+} and Mg^{2+}), and Flame Emission Spectrometry (Na^+, K^+, Ca^{2+} and SiO_2). Accuracy for major elements was better than ±5% (evaluated according to the following standards: Ion96-3 and LGC6020 (river waters) and diluted Li and B ICP-AES standard solutions (Merck)).

3.4. Sulfur isotope analysis

Sampling of the sulfur-rich minerals and karstic springs

Several sulfur-bearing minerals and dissolved species have been sampled to constrain the source of cave sulfate minerals, with:

i. 3 samples of cave gypsum coating the Ermite Cave walls;

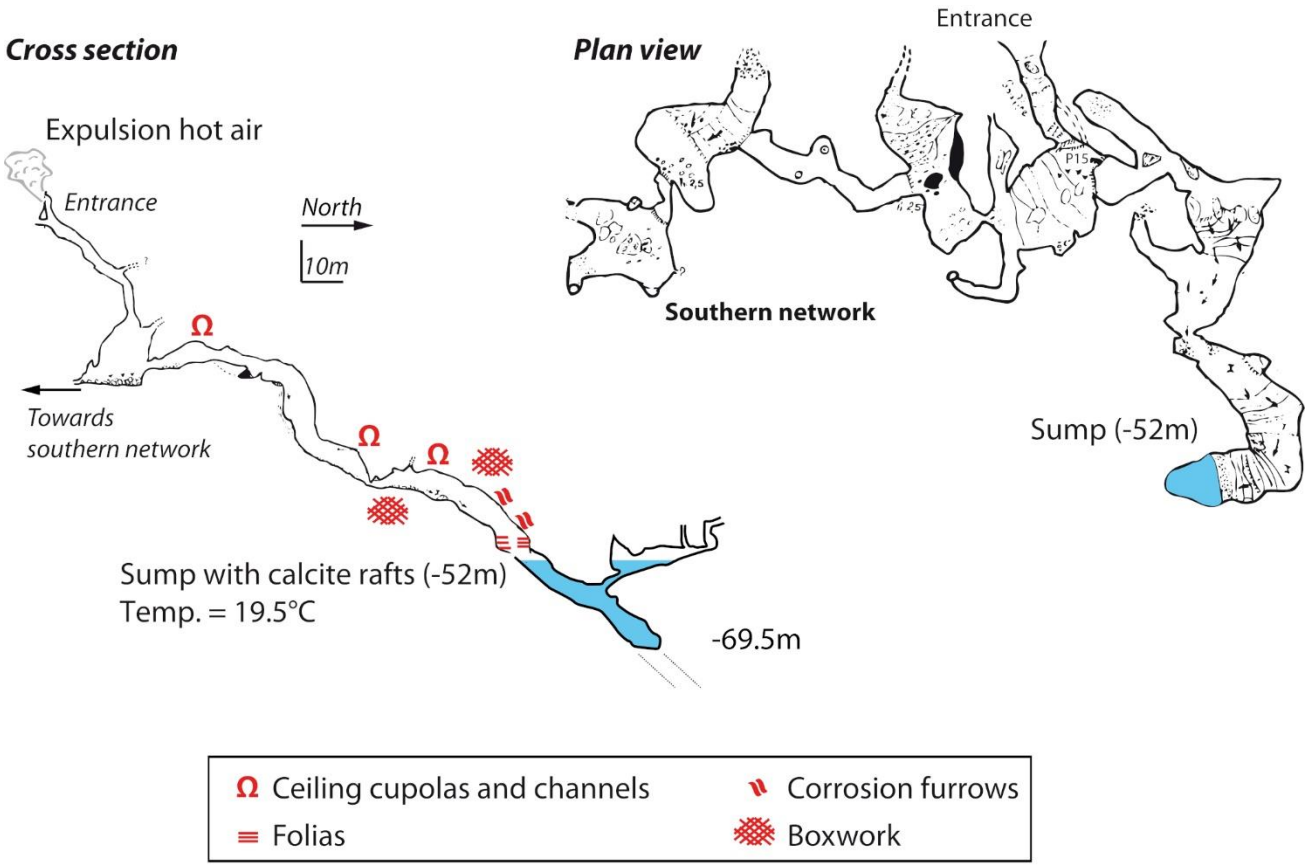

Figure 3: General architecture of the Vapeur Cave: vertical profile (left) and plan view (right) of the karstic networks with the type and position of all specific morphologies (ceiling cupolas and channels, corrosion furrows, boxworks) (topography provided by Spéléo Club du Haut Sabarthez).

ii. 3 powders of Aptian carbonates for trace sulfate mineral analysis in the Ermite Cave at various depths from the contact with cave gypsum (0.2 cm, 0.8 cm and 2.0 cm);
iii. gypsum and anhydrite deposits of the Triassic evaporitic series, with two samples in the Arignac underground quarry (Fig.1a for location);
iv. pyrite samples forming veins in Triassic gypsum in the Arignac quarry;
v. dissolved sulfates in the thermo-mineral water of the S9 borehole and in the thermal sumps of both Vapeur and Ermite Caves.

Sulfur isotopic composition is reported in the classical delta notation with respect to Vienna Cañon Diablo Troilite (V-CDT):

$$\delta^{x}S = (R_{sample}/R_{V\text{-}CDT} - 1) \times 1000 \quad (‰) \qquad (1)$$

with *x* = 34 and 33, where R is the ratio of the heavy to light isotopes ($^{x}S/^{32}S$).

To better visualize small isotopic composition deviations from the reference mass fractionation law between ^{32}S, ^{33}S and ^{34}S, we also used the capital delta values defined as:

$$\Delta^{33}S = \delta^{33}S - ((\delta^{34}S/1000 + 1)^{0.515} - 1) \times 1000 \ (‰) \qquad (2)$$

Major sulfur isotopes of trace sulfate minerals in carbonate rocks and dissolved SO_4^{2-}/H_2S in thermo-mineral springs

For trace sulfate minerals in limestones, about 10 mg of carbonate powder were treated similarly to Paris et al. (2014). Water samples were pretreated at the time of collection with ZnCl to precipitate reduced sulfur (H_2S) as ZnS. In the lab, samples were centrifugated to separate the precipitated ZnS. A 50 µl aliquot of the liquid phase was diluted in 1 ml of ultrapure water for sulfate concentration measurement on the Methrom Ion Chromatography System (ICS) and a 1 ml aliquot is taken for isotopic analyses. 1 ml of H_2O_2 30% was added to the ZnS solids and left at room temperature with a partially open lid for 1h and heated at 85 °C on a hot plate for 48h. The resulting solution was then centrifugated and the supernatant was recovered and used for ICS and isotopic measurement. $\delta^{34}S$ were measured on the ThermoScientific Neptune Plus

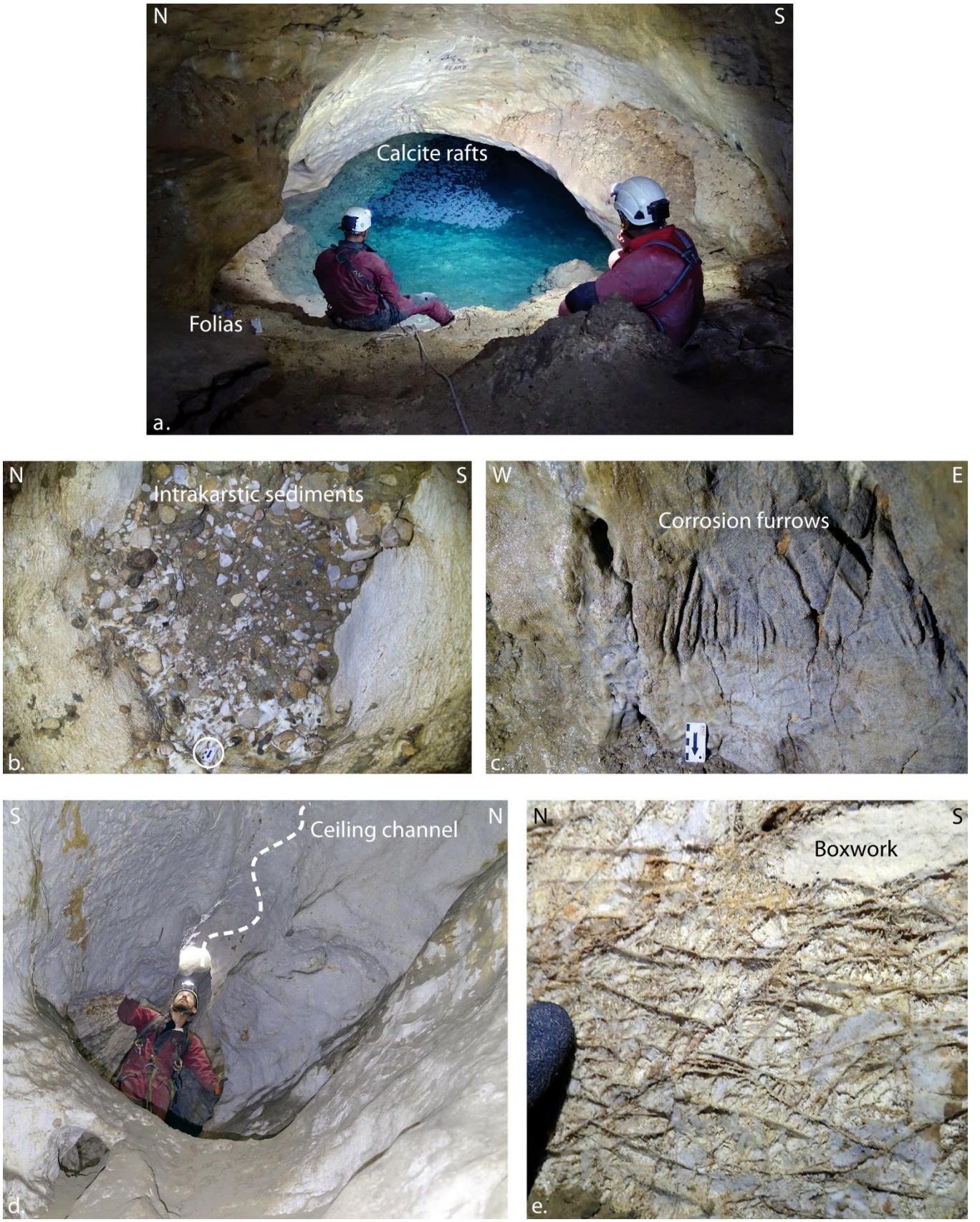

Figure 4: Photos of specific morphologies of the Vapeur Cave. a. Terminal thermal sump with calcite rafts at the surface. b. Ceiling cupolas coated by autochthonous carbonate fragments (15 to 20%) and allogenous metamorphic clasts conveyed by karstic fluvioglacial torrents (view of the ceiling; scale of 10 cm in the white circle). c. Corrosion furrows carving the cave wall (scale of 10 cm). d. Ceiling channel. e. Boxworks of sparitic veins on the gallery ceiling (view of the roof).

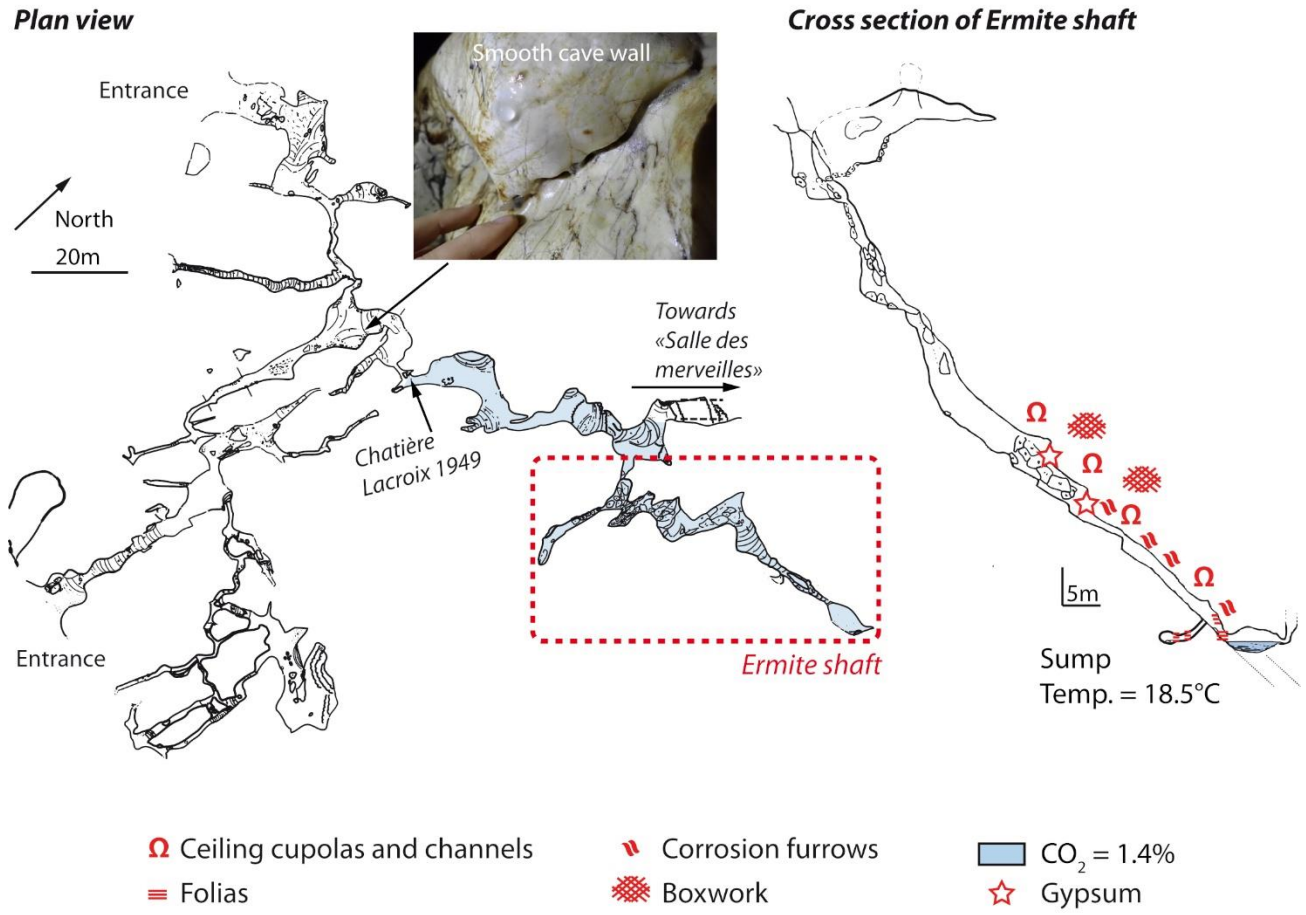

Figure 5: General architecture of the Ermite Cave: plan view (left) and vertical profile (right) of the network with the position of all specific morphologies (ceiling cupolas and channels, folia, corrosion furrows, boxworks), gypsum and area of abnormally high concentration of 1.4% of CO_2 (in blue) evidenced in the cave atmosphere (topography provided by Spéléo Club du Haut Sabarthez).

Multiple Collector – Inductively Coupled Plasma Mass Spectrometry (MC-ICPMS) at the Centre de Recherches Pétrographiques et Géochimiques (CRPG; Vandœuvre-les-Nancy, France) (Paris et al., 2013, 2014). Errors (2σ) were estimated at ±0.2‰ for both trace sulfate minerals and the dissolved sulfate/sulfide ions in thermo-mineral water based on a seawater long-term consistency standard.

Multiple sulfur isotopy (MSI) of cave sulfate minerals, sulfide minerals and evaporitic minerals

Multiple sulfur isotopes analyses ($\delta^{33}S$ and $\delta^{34}S$) were carried out at Institut de Physique du Globe de Paris (IPGP, France). A sulfur extraction from each powder was performed using either a Chromium Reduced Sulfides (CRS) solution (Canfield et al., 1986), or a Strongly Reducing Hydriodic Hypophosphorous acid solution (STRIP; as described in Kitayama et al., 2017) to extract sulfides and sulfates respectively. The H_2S released was then converted to Ag_2S by reaction with $AgNO_3$. Finally, a step of fluorination followed by purification steps using cryogenic traps and gas chromatography converted all the Ag_2S into SF_6 which was then analyzed by a ThermoFinnigan MAT 253 dual-inlet gas-source mass spectrometer (Sansjofre et al., 2016). Standard deviation corresponds to the sum of the internal and external errors possibly involved during extraction and fluorination procedures, and are c.a. 0.01‰ and 0.001‰ for $\delta^{34}S$ and $\Delta^{33}S$ values respectively (2σ).

3.5. Strontium isotopy of cave sulfate minerals

About 50 to 100 mg of powdered samples were prepared for strontium isotopic composition according to the method of Pin and Zalduegui (1997) at the Pôle de Spectrométrie Océan (PSO) in Brest (France). Sr isotopic compositions were measured in static mode on a Thermo TRITON. All measured Sr ratios were normalized to $^{86}Sr/^{88}Sr$ = 0.1194. During the course of analysis, Sr isotopic compositions of

standard solution NBS987 gave $^{87}Sr/^{86}Sr$ = 0.710270 ±0.000004 (2σ, n=7, recommended value 0.710250).

3.6. Oxygen isotopy of cave sulfate minerals

0.18 mg of 2 samples of cave gypsum were loaded into an autosampler of a TC/EA coupled to Isotopic Ratio Mass Spectrometry (IRMS) Delta plus xp Thermofisher for the oxygen isotopic composition measurement (combustion temperature of 1450 °C) at the Scientific and Technical Centers of the Universitat de Barcelona (Spain). We used the classical delta notation in ‰ with respect to V-SMOW (Vienna Standard Mean Ocean Water) and V-PDB (Vienna Pee Dee Belemnite). The reference standards used were NBS-127 ($\delta^{18}O$ value of +8.59‰), UB-ASC ($\delta^{18}O$ value of +13.2‰), UB-YCEM ($\delta^{18}O$ value of +17.6‰) and IAEA-SO6 ($\delta^{18}O$ value of -11.4‰) for an obtained standard deviation inferior to 0.2‰.

3.7. Oxygen, hydrogen and strontium isotopes of water

Oxygen and hydrogen isotope measurements were performed at BRGM stable isotope laboratory (France) by equilibrating during one night 1 mL of water with gas mixtures of H_2–He and CO_2–He respectively for δD and $\delta^{18}O$, and using a Finnigan MAT 252 mass spectrometer (Assayag et al., 2008). The external precision was ±0.1‰ for $\delta^{18}O$ and ±0.8‰ for δD V-SMOW.

Preparation of water samples for strontium isotopic composition was made according to method of Pin and Bassin (1992). 150 ng of Sr were analyzed using a Finnigan MAT 262 multi-collector mass spectrometer at BRGM's stable isotope laboratory. The $^{87}Sr/^{86}Sr$ values were normalized to the certified value of the NBS987 standard 0.710240. An average internal precision of ±10 ppm (2σ) was obtained and the reproducibility of the $^{87}Sr/^{86}Sr$ ratio measurements was verified by repeated analysis of the NBS987 standard ($^{87}Sr/^{86}Sr$ = 0.710243 ±10, 2σ).

3.8. Oxygen and carbon isotopes of carbonates

For carbon and oxygen isotopic compositions of calcite (rafts, folia and unaltered host rock), an aliquot of each sample between 1 to 100 mg of powder was reacted with 2 mL of supersaturated orthophosphoric acid at 70 °C for at least 10h under a He atmosphere. Carbon and oxygen isotopic compositions of the produced CO_2 were then measured with a Thermo Scientific MAT 253 continuous flow isotope ratio mass spectrometer at CRPG. Values are reported to the delta notation in ‰ relative to V-PDB for carbon isotopes, and to V-SMOW and V-PDB for oxygen isotopes of water and mineral respectively. All sample measurements were adjusted to the internal reference calibrated on the international standards IAEA CO-1, IAEA CO-8 and NBS 19. The reproducibility was better than 0.2‰ (2σ).

4. Results

4.1. Cave hydrology and specific morphologies and minerals

The Vapeur Cave

The Vapeur Cave opens at the foot of an Urgonian cliff at an altitude of 560 m, about 70 m above the current Ariège River. It includes 3 main vertical shafts linked together by sub-horizontal galleries, for a total development of 270 m (Fig.3). The deeper shaft reaches a thermal sump at a depth of -52 m from the entrance (Fig.4a), with a diving exploration and topography down to -69.5 m, *i.e.* 17.5 m below water level. This cave has been defined as a "smoking shaft" (Audra, 2017), evidenced by a condensation plume visible at the cave entrance during cold days.

In terms of specific minerals, calcite rafts have precipitated at the thermal water surface (Fig.4a). Considering particular morphologies, pluri-dm to metric symmetrical cupolas on the ceiling are present all along the network, sometimes coated by detrital materials (c.a. 15 to 20% of autochthonous carbonate clasts, and allogenous clays and pebbles of metamorphic origin with significant concentration of iron) (Fig.4b). The most intensive corrosion features are observed in the first 20 m above the current water table with pluri-cm-deep corrosion furrows and karren developing from the ceiling to the floor, and converging toward the water surface (Fig.4c). Pluri-dm-deep ceiling channels (Fig.4d) and numerous boxworks with sparitic veins in relief (Fig.4e), due to the preferential dissolution of the micritic matrix of the Urgonian limestone, are also observed. *In-situ* measurements using GA5000 gas analyzer revealed no significant gas concentration anomalies (CO_2 or H_2S) in the cave atmosphere (analysis made during July 2018).

The Ermite Cave

The two main entrances of the Ermite Cave open at the same Urgonian cliff as the Vapeur Cave, at an altitude of 550 m, about 60 m above the Ariège river. The cave is composed of two superposed levels with distinct morphologies, for a total development of

Figure 6: Photo of the bottom part of the Ermite Cave showing ceiling channels rising above the terminal thermal sump, corrosion furrows on the walls, and a close-up view of folia.

900 m (Fig.5). The upper network (250 m of development) shows an alternation of horizontal galleries with successive low passages (around 1 m-high, 1 to 2m-wide) and chambers (between 3 and 6 m-high, 2 to 4 m-wide). Cave walls of this part are very smooth, shiny, intensely polished (Fig.5), with local preservations of clastic infillings cemented by calcitic cements (similar to the Vapeur cave sediments).

The lower network includes shafts and inclined galleries (1 to 5 m-high and 2 to 5 m-wide) that follow the bedding plane down to a thermal sump at a depth of around 70 m below the entrances. Various corrosion structures and speleothems are observed above this sump:

i. Sinuous ceiling channels, with very curved walls devoid of concretions, starting from the sump and rising along the roof up to 8 m above the water table (Fig.6);
ii. Deeply incised ceiling cupolas develop along the ceiling channels (Fig.7a and 7b). Some of them are coated with brown-colored iron- and manganese-rich incrustations delimiting horizontal levels. Such levels mark the former water-air interface of trapped air pockets;
iii. Folia are observed few meters above the water table (Fig.6 and 7c). Folia appear as typical 3 to 20 cm-long forms of inverted cups forming amalgamated “fungi-like” texture similar to the “bracket fungi” fabric commonly described in the literature (e.g. Audra et al., 2009; D’Angeli et al., 2015; Lopez-Martinez et al., 2020);
iv. As also observed in the Vapeur Cave, thin and vertical corrosion furrows incise the majority of Urgonian walls and floors in the first 10 m above the sump. Furrows are spaced each other from 1 to 20 cm and converge toward the sump (Fig.6 and 7d);
v. Walls and roofs are locally encrusted with old calcitic crusts, characterized by a patchy geometry. Theses crusts are highly corroded and some of them are clearly incised by the vertical corrosion furrows (Fig.7d);
vi. Higher in the gallery, more than 15 m above the sump, all the walls, ceilings and laminated karstic sediments are highly corroded (Fig.7e) with the development of small pluri-centimetric cups systematically coated by iron-rich calcite

crusts, and sometimes exhibiting a popcorn-like texture;

vii. Several generations of cm-thick gypsum crusts develop in the upper part of the lower network, at the level of very polished incurved surface at the head of vertical conduits (Fig.7f). They are sometimes separated from each other by calcitic laminae or silty/clayey material (Fig.8a and 8b). In small cavities or fractures enlarged by corrosion, we also observed secondary gypsum blisters (hemispherical to nearly spherical speleothem on the cave wall; Fig.8c) and very fine needles (Fig.8d) coating prior gypsum crusts and clayey coatings. DRIFT and DRX analyses did not reveal other sulfate species than pure gypsum. No alteration is visible at the contact between gypsum and host carbonate rock, even using microscopic observations.

Table 1: Physico-chemical characteristics of the S9 borehole thermo-mineral water (measurements performed the 26/04/2005 and 22/10/2008; Antea, 2009) and of the Ermite and Vapeur caves sump water (this study).

	S9 borehole thermal water (Antea, 2009)	Vapeur Cave groundwater (this study)	Ermite Cave groundwater (this study)
Physical properties			
Temperature (°C)	52/59	19.5	18.5
pH	6.5/7.6	7.44 in situ/7.65 lab	7.29 in situ/6.45 lab
Conductivity (µS/cm)	1751/1885	454	486
Chemical composition (mg/l)			
Na^+	38/46	<2	<2
K^+	7.9	<2	<2
Ca^{2+}	375/407	63.4	68
Mg^{2+}	57/69	3.4	5.6
O_2	0.8	8.32	7.81
Fe^{2+}	< L.D	< L.D	< L.D
SO_4^{2-}	1020/1300	18.6	27.4
H_2S	< L.D	< L.D	< L.D
Cl^-	45/53	2.9	2.35
HCO_3^-	126/150	289.4	290.9
NO_3^-	<1	< L.D	< L.D
Organic ions	< L.D	< L.D	< L.D

According to *in-situ* gas measurements in the Ermite Cave, deeper parts of the network (below the narrow passage separating the lower and upper networks; the "Châtière Lacroix 1949"; Fig.5) were characterized by a significant CO_2 concentration in the atmosphere, depending on the season: a proportion of 1.4% of CO_2, associated to an oxygen depletion (19.8% instead of 20.1%) during the summer 2018 (July), and 0.7% of CO_2 during the winter 2019 (January).

4.2. Physico-chemistry and isotopy of thermo-mineral waters and cave minerals

Physico-chemistry of thermo-mineral waters

Physical parameters of both cave sump waters (this study), as well as for the S9 borehole water (Antea, 2009), are synthesized in the Table 1. Physical data and chemical composition of the sump waters are similar between both caves. During summer 2018, we measured water temperatures of 18.5 °C and 19.5 °C respectively for the Ermite and the Vapeur warm sumps. These values are higher than the 10 to 12 °C measured in surface water. For the Ermite and Vapeur caves respectively, pH are 7.29 and 7.44, while conductivities are 486 and 454 µS/cm. Ionic concentrations are also similar between both waters, with relatively low contents of chloride ions (Ermite Cave: 2.35 mg/l; Vapeur Cave: 2.9 mg/l) and sulfate ions (Ermite Cave: 27.4 mg/l; Vapeur Cave: 18.6 mg/l). Potassium, sodium and magnesium concentrations are very low, below 2 mg/l. The content of dissolved H_2S is negligible with a value lower than 10^{-2} mg/l. The concentration in bicarbonate ions is of 290.9 mg/l for the Ermite Cave, and 289.4 mg/l for the Vapeur Cave. Dissolved oxygen concentration is similar between both caves with values of 7.81 mg/l in the Ermite Cave and 8.32 mg/l in the Vapeur Cave, which is a common content for superficial water. During investigations in the Ermite cave, in fall 2018, ephemeral strings of bubbles rose from the warm sump. Unfortunately, due to the transient nature of these emissions and their awkward access, we were not able to sample these gases for chemical analysis.

Isotopic composition

All isotope results are synthesized in Table 2.

Calcite close to the sump water of Ermite and Vapeur caves

Results show negative carbon and oxygen isotopic signatures for calcite concretions close to the sump water surface, with a $\delta^{13}C$ values of -6.7 and -6.6 ±0.2‰ V-PDB, and $\delta^{18}O$ values of -9.6 and -11.0 ±0.2‰ V-PDB

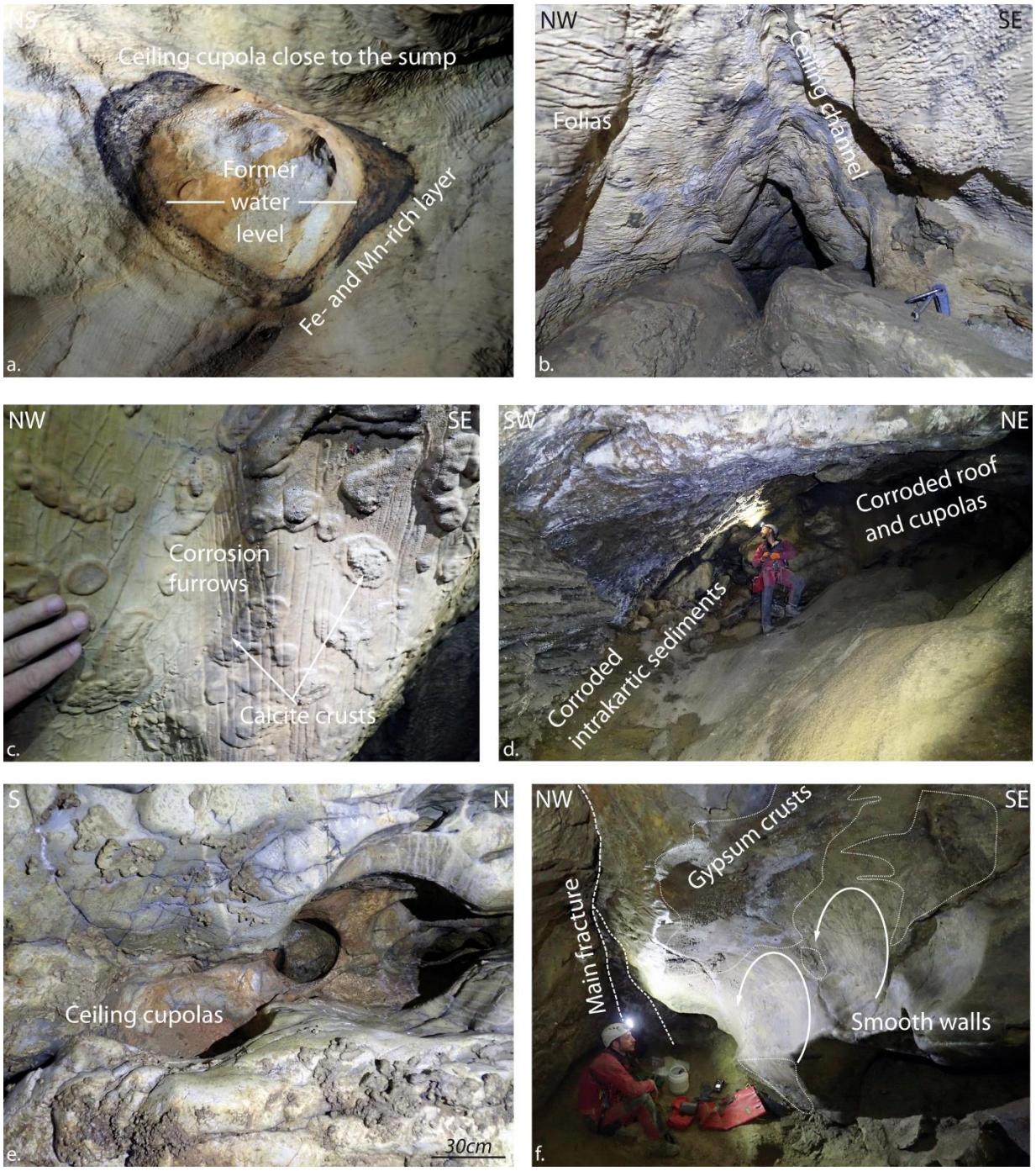

Figure 7: Photos of specific morphologies of the Ermite Cave. a. Ceiling cupolas with an iron- and manganese-rich layer at the base marking a former water-air interface of trapped air pockets. b. Ceiling interpenetrated cupolas (view of the roof). c. Ceiling channel close to the sump and close-up view of folia on the wall (photo by J-Y. Bigot). d. Corrosion furrows carving the limestone wall, karstic sediments and calcite crust. e. View of an intensively corroded gallery with significant alteration of ceiling, walls and karstic sediments (close-up view of corrosion cups). f. Smooth walls in convection niches coated by gypsum crusts at the top of a more vertical shaft and along a main fault plane.

for the Ermite Cave (calcite forming folia); and $\delta^{13}C$ values of -7.3 ±0.2‰ V-PDB, and a $\delta^{18}O$ values of -10.4 ±0.2‰ V-PDB for the Vapeur Cave (calcite rafts on warm water surface) (Fig.9a). The unaltered Urgonian host rock is characterized by a positive value for $\delta^{13}C$ of +0.3 ±0.2‰ V-PDB, and negative for $\delta^{18}O$ of -15.2 ±0.2‰ V-PDB.

Thermo-mineral waters

The signatures in $\delta^{18}O$ and δD for the sump water of the Ermite Cave are -9.9 ±0.1‰ V-SMOW and -67.1 ±0.8‰ V-SMOW respectively; and for the Vapeur Cave of -9.6 ±0.1‰ V-SMOW and -65.5 ±0.8‰ V-SMOW (Fig.9b). The $^{87}Sr/^{86}Sr$ ratios in waters are 0.707853

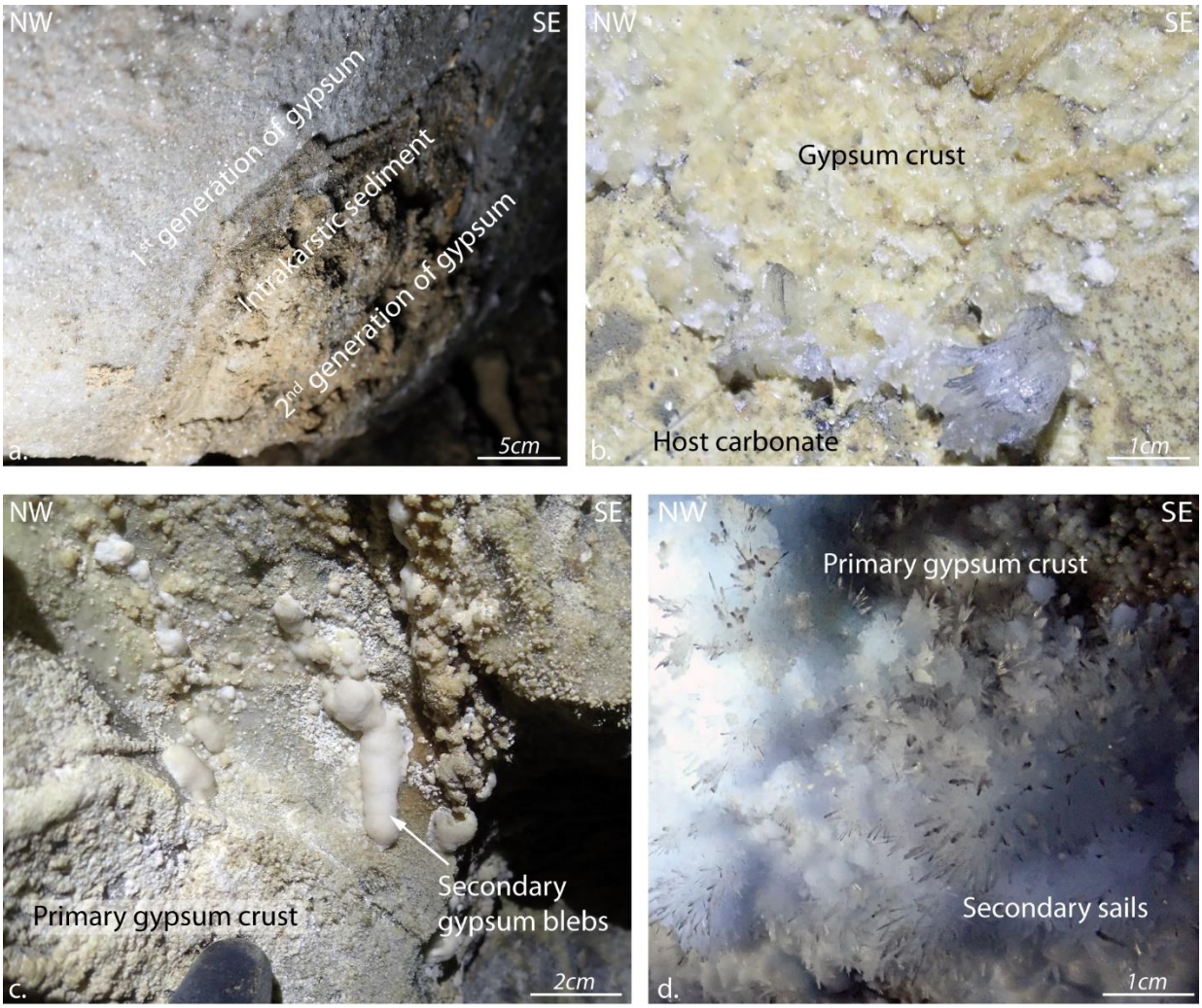

Figure 8: Photos of gypsum precipitates in the Ermite Cave. a. Two generations of gypsum crusts separated by a layer of clay-rich karstic sediments. b. Detailed view of the gypsum crust resting directly on the host limestone. c. Secondary gypsum blisters resting on the primary massive gypsum crust. d. Secondary fine gypsum needles on primary gypsum crust.

±0.000007 and 0.707926 ±0.000006 for the Ermite Cave and the Vapeur Cave, respectively. The sulfur isotopic signatures of the dissolved sulfate ions are again close to each other, with a $\delta^{34}S$ (SO_4^{2-}) values of +6.1 ±0.2‰ V-CDT for the Ermite sump, and of +4.9 ±0.2‰ V-CDT for the Vapeur sump. Finally, the thermo-mineral water of the S9 borehole is characterized by $\delta^{34}S$ value of dissolved sulfate ions of +14.8 ±0.2‰ V-CDT (Fig.10).

Ermite Cave gypsum

The $^{87}Sr/^{86}Sr$ values of gypsum sampled in the Ermite cave are quite similar to those of the sump water of this same cave, with slightly higher values of 0.708197 ±0.000006 and 0.708291 ±0.000008. Cave gypsum show negative MSI values: Erm1 with $\delta^{34}S$ value of -3.56 ±0.008‰ V-CDT and $\Delta^{33}S$ value of -0.004 ±0.007‰, Erm2 with $\delta^{34}S$ value of -5.06 ±0.010‰ V-CDT and $\Delta^{33}S$ value of -0.034 ±0.013‰, and Erm3 with $\delta^{34}S$ value of -7.33 ±0.008‰ V-CDT and $\Delta^{33}S$ value of -0.043 ±0.014‰ (Fig.10). $\delta^{18}O$ values of Erm2 and Erm3 are -0.6 ±0.2‰ V-SMOW and +0.6 ±0.2‰ V-SMOW respectively.

Pyrites, gypsum and anhydrite of Triassic evaporitic series

Triassic evaporitic minerals of the Arignac underground quarry (Fig.1a for location) are characterized by respective $\delta^{34}S$ and $\Delta^{33}S$ values of +17.38 ±0.005‰ V-CDT and of -0.001 ±0.011‰ for gypsum, and +15.34 ±0.010‰ V-CDT and +0.008 ±0.013‰ for anhydrite (Fig.10). Pyrites precipitated in Triassic gypsum are characterized by lower sulfur isotopic signature with $\delta^{34}S$ values of +1.66 ±0.008‰ V-CDT and +2.09 ±0.003‰ V-CDT, and $\Delta^{33}S$ values of -0.003 ±0.008‰ and -0.010 ±0.010‰.

Table 2: Results of multiple sulfur, strontium, oxygen, carbon and hydrogen isotopy in: Ermite and Vapeur caves sump thermal water, calcitic speleothems, cave sulfates (massive gypsum crusts and trace sulfate minerals in host limestone), Triassic gypsum/anhydrite/pyrite, and thermo-mineral water of the S9 borehole.

Water/ mineral		$\delta^{34}S$ ‰ V-CDT	Error ‰	$\Delta^{33}S$ ‰	Error ‰	$^{87}Sr/^{86}Sr$	Error	δD ‰ V-SMOW	Error ‰	$\delta^{18}O$ ‰	Error ‰	$\delta^{13}C$ ‰ V-PDB	Error ‰
Ermite Cave													
Thermal water		Sulfates +6.1	0.2			0.707853	$7.\ 10^{-6}$	-67.1	0.8	-9.9 V-SMOW	0.1		
Calcite (folia)										-11.0	0.2	-6.7	0.2
										-9.6 V-PDB	0.2	-6.6	0.2
Host Limestone										-15.2 V-PDB	0.2	+0.3	0.2
Trace sulfates in host rock*	0.2cm	-9.5	0.2										
	0.8cm	-2.6	0.2										
	2cm	+9.3	0.2										
Gypsum	Erm1	-3.56	0.008	-0.004	0.007	0.708197	$6.\ 10^{-6}$				0.2		
	Erm2	-5.06	0.010	-0.034	0.013	0.708291	$8.\ 10^{-6}$			-0.6	0.2		
	Erm3	-7.33	0.008	-0.043	0.014					+0.6 V-SMOW			
Vapeur Cave													
Thermal water		Sulfates+4.9				0.707926	$6.\ 10^{-6}$	-65.5		-9.6 V-SMOW	0.1		
Calcite rafts										-10.44 V-PDB	0.2	-7.3	0.2
Triassic formation (Arignac underground quarry)													
Gypsum		+17.38	0.005	-0.001	0.011								
Anhydrite		+15.34	0.010	+0.008	0.013								
Pyrite		+1.66	0.008	-0.003	0.008								
		+2.09	0.003	-0.010	0.010								
Thermal water in S9 borehole													
Sulfate ions		+14.8	0.2										

*(from gypsum interface)

Trace sulfate minerals in host Urgonian limestone of the Ermite Cave

The transect of trace sulfate minerals contained within Urgonian limestone on the wall of the Ermite Cave shows $\delta^{34}S$ values ranging from -9.5 ±0.2‰ V-CDT at 2 mm from the gypsum-carbonate interface to -2.6 ±0.2‰ V-CDT at 0.8 mm, and finally +9.3 ±0.2‰ V-CDT at 2.0 cm depth (Fig.11).

5. Discussion

5.1. Geomorphological evidences of recent to active hypogenic condensation-corrosion

Warm sumps, the CO_2-rich Ermite Cave atmosphere and the occurrence of rising bubbles are clear evidences for an ongoing hydrothermal activity rising in the caves, where deep hydrothermal inputs mixes with superficial meteoric water infiltrations. In hypogenic carbonic caves, CO_2 ascent commonly causes the formation of calcitic folia and rafts related to thermo-mineral water degassing (e.g. Audra et al., 2009; Lopez-Martinez et al., 2020), which is also observed in both Vapeur and Ermite caves. Though CO_2 degassing can occur underwater or at the air-water interface, the absence of bubble trails, formed from CO_2 pressure decrease in water (Audra et al., 2009), is rather in favor of CO_2 degassing at the water surface directly to the cave atmosphere. For example, in the Movile Cave (Romania), the main karstification mechanism is attributed to the carbonic condensation-corrosion processes associated with an atypical CO_2 proportion of 1.5% in the atmosphere and an oxygen depletion with a proportion between 19.5 and 20% (Sarbu and Lascu, 1997). This CO_2 content is comparable to the summer values we measured in the Ermite Cave. Within both Ermite and Vapeur caves, dissolution features observed above the warm sumps

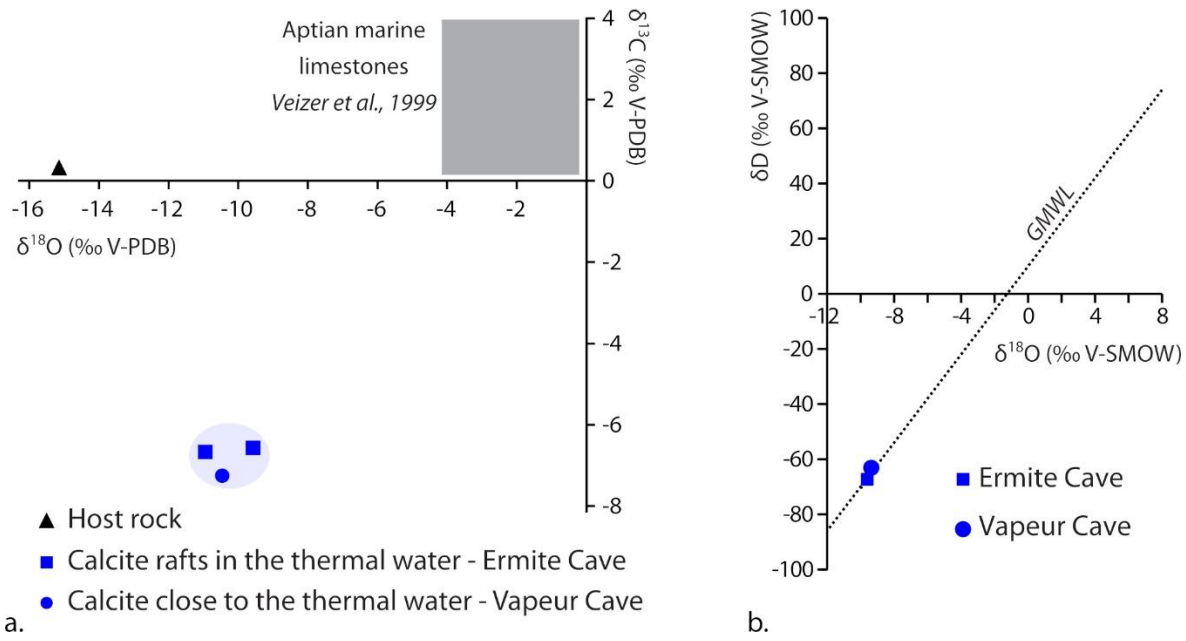

Figure 9: a. $\delta^{13}C$ vs. $\delta^{18}O$ graph of the host limestone and calcite precipitated from the degassing of thermal sumps in the studied caves (calcite rafts in the Vapeur Cave and folia in the Ermite Cave). The signature of Aptian marine limestone is reported in the grey rectangle (Veizer et al., 1999). b. δD vs. $\delta^{18}O$ graph of the sump waters in both the Ermite and Vapeur caves. The Global Meteoric Water Line (GMWL) is reported in black (Craig, 1961).

are typical of condensation-corrosion processes in thermally-influenced atmosphere because of a thermal gradient between the pool of warm water and the "colder" host rock (e.g. Dublyansky and Dublyansky, 2000; Dreybrodt et al., 2005; Audra et al., 2009). During this process, CO_2 from the cave atmosphere is dissolved at the contact with condensation water film covering the cave wall to form carbonic acid, while H_2S is oxidized in the condensate to produce sulfuric acid, and both reactions thus contribute to the intense dissolution of the carbonate host rock (e.g. Sarbu and Lascu 1997; Audra et al., 2007a).

Alteration features in such hypogene karstification processes depend on the degree of condensation on the wall (as also observed in the Chevalley Aven; Audra et al., 2007a). In both caves, from the warm sump surface, rising vapor leads to a more intense condensation-corrosion on the ceiling due to a strong thermal gradient, at the origin of several “condensation channels” (Fig.4d and 6). Even if channels formed at the ceiling could be attributed to convection cells in a phreatic condition (Klimchouk, 2007), other authors demonstrated that such morphologies can also result from the condensation-corrosion linked to rising warm air (Audra, 2007; Audra et al., 2007a; Temovski et al., 2013). Just below condensation channels, numerous corrosion furrows (Fig.6 and 7c) probably formed from the runoff of carbonic acid-rich water film along the cave walls (e.g. Cigna and Forti, 1986), which is consistent with ceiling channel with a condensational origin. At the top of the shaft and along main fracture planes in the Ermite Cave, hot air convection, favored by the mixing between ascending warm air and descending cold air, induces a more intense condensation leading to a greater corrosion and wall smoothing than in the narrower underlying conduits, forming a kind of air convection niches (Fig.7f). These features appear very similar to the “*solution-smoothed walls*” presented by Dublyansky and Spötl (2014), which are also associated to hypogenic condensation-corrosion process. These niches probably formed initially during an older stage of the cave development and were reactivated very recently, as they are covered by Quaternary detrital materials. This observation confirms that the recent and still active carbonic hypogenic event reworked the preexistent morphologies. Crusts of iron-rich calcite and aragonite developed on those polished niche surfaces and were linked to the supersaturation of condensation water enriched in calcium and bicarbonate ions during the dissolution by carbonic acid, where iron derived from the alteration of cave sediments by carbonic and sulfuric vapors. Gypsum crusts also precipitated at the surface of these convection niches. Such cave sulfate minerals can be related to the sulfuric acid action on

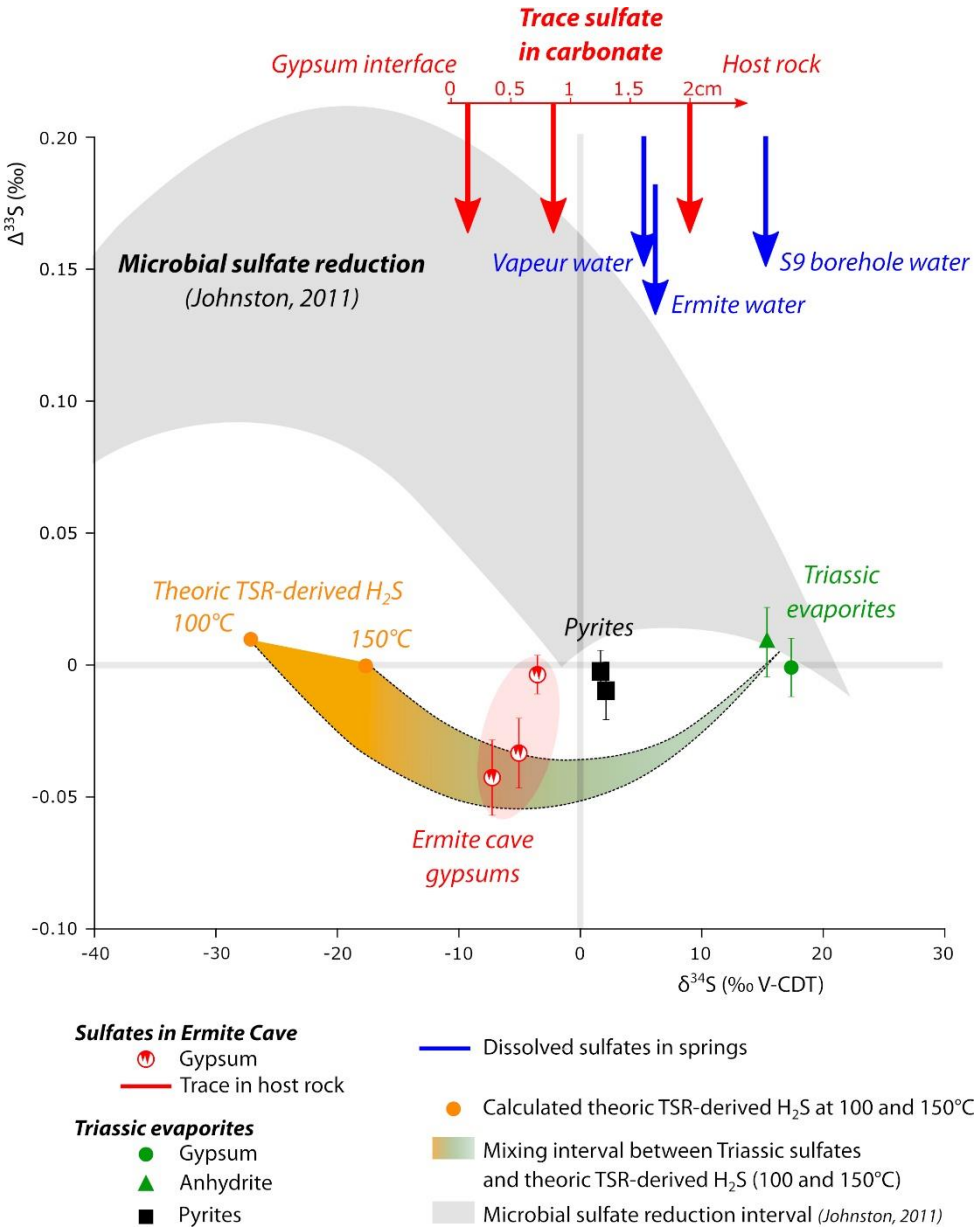

Figure 10: Multiple sulfur isotopes (MSI; $\delta^{34}S$ vs. $\Delta^{33}S$) diagram with all the sulfur species potentially implied in the Ermite Cave gypsum precipitation (see the legend below the graph). Vertical arrows at the top of the diagram indicate MSI values where the $\delta^{34}S$ is precise but the error of $\Delta^{33}S$ is superior to 0.3‰. The grey area corresponds to the Microbial Sulfate Reduction (MSR) zone defined in Johnston (2011). The curved gradient interval corresponds to the mixing curves (*i.e.* relative contribution) between the Triassic evaporitic sulfate ions in hydrothermal water and the theoretic deep TSR-derived H_2S respectively generated at 100, 125 and 150 °C (see text for explanation).

the carbonate rock. The potential involvement of SAS will be discussed in the next paragraph in the light of the MSI results.

If hypogenic condensation-corrosion is predominant on the gallery ceiling, the lower part of the rooms is the site of evaporation-deposition (e.g. Audra et al., 2007a). This stratification of evaporation-deposition is the result of the air circulation in the cave, as, particularly during winter, the cold air descends along the inclined floor, and expels the hot air above the sump, which rises along the ceilings (ceiling channels). Just below condensation channels and in the largest rooms, dripping of water enriched in carbonic acid induced an intense corrosion of karstic sediments affected by the development of small cups and iron-rich calcite crusts (Fig.7d). These crusts result from the supersaturation and evaporation of the bicarbonate-rich condensation water. Popcorn calcites also crystallized from supersaturated hydroaerosol decantation during the evaporation (Dublyansky and Pashenko, 1997; Hill and Forti 1997; Dublyansky, 2000;

Audra et al., 2009). This particularly aggressive runoff of condensation water was probably responsible for the dissolution of the first generation of gypsum, which subsequently reprecipitated by evaporation in the form of blisters and needles coating the primary gypsum crusts (e.g. Klimchouk et al., 2017; Fig.8c and 8d).

5.2. Source of sulfur for cave sulfate minerals and implication for speleogenesis

Current hydrothermal leaching of Triassic evaporites at depth

The main sulfur sources in the Tarascon-sur-Ariège basin are the Triassic evaporites present at depth. The latter form salt diapirs that outcrop in the northern part of the basin (Fig.1a) but is present at a depth around 1000 m below the studied caves. Before the water capture by the S9 borehole (1996), the thermal facilities were supplied by hot waters flushing both the Ariège fluvial sediments and surrounding Urgonian carbonate rocks. The rising hydrothermal water migrates today within the fractured and karstified Jurassic and Cretaceous carbonate formations (Fig.1b). The high contents in dissolved sulfates (between 1120 and 1300 mg/l; Antea, 2009; Table 1) and chlorides (between 45 and 53 mg/l; Antea, 2009; Table 1) measured in the S9 borehole waters suggest a hydrothermal leaching of Triassic evaporites at depth. This is confirmed by the similarity of $\delta^{34}S$ signatures between sulfate ions in the thermo-mineral water (+14.8 ±0.02‰ V-CDT) and Triassic evaporitic minerals sampled at the Arignac quarry (+17.38 ±0.005‰ V-CDT for gypsum and +15.34 ±0.01‰ V-CDT for anhydrite) (Fig.10).

It is likely that the warm waters of both Vapeur and Ermite sumps are at least partially supplied by the same hydrothermal circulation since they display very similar chemical composition. Hydrogen and oxygen isotopes suggest that their main water supply is of meteoric origin (Ermite Cave: $\delta^{18}O$ value of -9.9 ±0.1‰ V-SMOW and δD value of -67.1 ±0.8‰ V-SMOW; Vapeur Cave: $\delta^{18}O$ value of -9.6 ±0.1‰ V-SMOW and δD value of -65.5 ±0.8‰ V-SMOW; on the Global Meteoric Water line, Craig (1961); Fig.9b), probably through infiltrations at depth via the inverted faults bordering the Paleozoic basement to the east and the west of the Ariège Valley. Thermal water then rose up to the cave according to regional thermal convection loops (Fig.1b). $^{87}Sr/^{86}Sr$ values of these sump waters (0.707853 ±0.000007 for Ermite Cave and 0.707926 ±0.000006 for Vapeur Cave) are also similar to the Triassic evaporites (between 0.70745 and 0.70795 after Koepnick et al. (1990) and up to 0.7086 after Song et al. (2015)), confirming the deep connection with the underlying Triassic salts through hydrothermal circulation. The low content of sulfate ions in cave sump water can be explained by the fact that this water is diluted by lateral meteoric inputs, especially from the Ariège valley groundwater stored in alluvium, while the water in the S9 borehole was sampled below the mixing zone with meteoric water, explaining a higher sulfate concentration.

A thermochemical production of H_2S at depth

Considering the magnitude order of natural variation of strontium isotopic composition, the $^{87}Sr/^{86}Sr$ of Ermite Cave gypsum (0.708197 ±0.000006 and 0.708291 ±0.000008) is similar to the strontium isotopic signatures of cave sump waters (0.707853 ±0.000007 for Ermite Cave and 0.707926 ±0.000006 for Vapeur Cave) and those of the Triassic evaporites (Koepnick et al., 1990; Song et al., 2015). Therefore, our data are consistent with hydrothermal fluid being responsible for the precipitation of the Ermite Cave gypsum. In addition, $\delta^{18}O$ values of bulk gypsum sampled in the Ermite Cave gives information on the source of oxygen during cave sulfate precipitation and oxidation of H_2S (e.g. Onac et al., 2011; Temovski et al., 2018). Two possible oxygen sources are: (i) atmospheric oxygen O_2 (mean $\delta^{18}O$ value of +23.8‰ V-SMOW; Horibe et al., 1973), and (ii) the H_2O in underground water ($\delta^{18}O$ of -9.9 ±0.1‰ V-SMOW for the Ermite Cave at the time of water sampling, even if it can vary over time during climate changes). Considering the oxygen isotope enrichment factor between sulfate and atmospheric oxygen ($\varepsilon^{18}_{SO4-O2}$) or water ($\varepsilon^{18}_{SO4-H2O}$), which varies between 0 and -11.4‰ V-SMOW for $O_{2(g)}$ and between 0 and +9.7‰ V-SMOW for the H_2O (Van Stempvoort and Krouse, 1994), oxygen in the Ermite Cave gypsum ($\delta^{18}O$ values of -0.6 and +0.6 ±0.2‰ V-SMOW) mostly derived from the cave sump water (between 69 and 100% of contribution), possibly during evaporation-condensation.

However, the $\delta^{34}S$ values of sulfate ions dissolved within both cave sumps (+6.1 ±0.2‰ V-CDT for Ermite Cave and +4.9 ±0.2‰ V-CDT for Vapeur Cave) are different from those measured in Triassic evaporites (+15.34 ±0.01 and +17.38 ±0.005‰ V-CDT) and also in the S9 borehole water (+14.8 ±0.2‰ V-CDT) (Fig.10). This difference in sulfur isotopic signatures does not support precipitation by supersaturation of sulfates from the warm water, which would rather induce negligible fractionation and thus similar $\delta^{34}S$ values (Raab and Spiro, 1991). In addition, the absence of

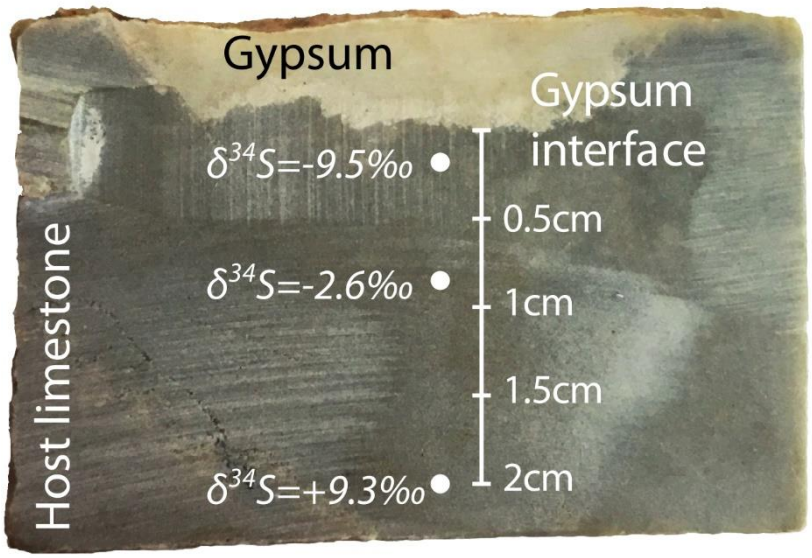

Figure 11: Photo of the interface between cave gypsum and host limestone in the Ermite Cave, indicating the position of samples and $\delta^{34}S$ values (in ‰ V-CDT) of trace sulfate minerals used to identify the carbonate-gypsum substitution front.

pyrite in the cave host rock also excludes the impact of local pyrite oxidation in the precipitation of gypsum.

Large fractionation of $\delta^{34}S$ values observed between cave gypsum, cave dissolved sulfate ions and Triassic evaporites ($\Delta^{34}S_{\text{Triassic evaporites-gypsum}}$ values between 18.87 and 24.66‰ and $\Delta^{34}S_{\text{Triassic evaporites-dissolved sulfates}}$ values between 9.24 and 12.48‰) is commonly associated with sulfate reduction (reaction $SO_4^{2-} \rightarrow H_2S$), either Microbial Sulfate Reduction (MSR, below 80 °C; Machel et al., 1995; Machel, 2001; Farquhar et al., 2003; Johnston, 2011) or Thermochemical Sulfate Reaction (TSR, above 100 °C; Heydari and Moore, 1989; Worden and Smalley, 1996; Machel, 2001; Cai et al., 2003). In both reactions, cave gypsum finally results from the oxidation of ^{34}S-depleted H_2S, and is thus necessarily derived from the production of sulfuric acid, as opposed to reprecipitation of previously dissolved gypsum. Given that MSR and TSR are associated with distinct fractionation of $\delta^{33}S$ and $\delta^{34}S$ values, negative values of $\Delta^{33}S$ for Ermite Cave gypsum (between -0.004 and -0.043‰; Fig.10) confirms the TSR and exclude the MSR, the latter instead implying: (i) an increase in $\Delta^{33}S$ values up to +0.2 ‰ compared to the initial sulfates (see the MSR grey interval in Fig.10; Farquhar et al., 2007; Johnston et al., 2007), and (ii) a higher fractionation of $\delta^{34}S$ with value up to +72‰ (Machel et al., 1995; Wortmann et al., 2001; Farquhar et al., 2007; Johnston, 2011; Sim et al., 2011). Moreover, no such a bacterial activity is evidenced in the caves as neither filaments on cave walls (using ultraviolet observations) nor superficial microbially-derived H_2S has been observed. Sulfate reduction is typically associated with significant amounts of organic matter which act as an electron donor for the reaction to occur. At the scale of the sedimentary basin, the possible sources for organic matter are the Middle to Late Liassic marly limestones at depth. Indeed, these sediments constitute one of the main petroleum source rocks in the Northern Pyrenees and South Aquitaine Basin (Connan and Lacrampe-Couloume, 1993; Biteau et al., 2006). Liassic series are now buried between 600 and 1500 m in the studied basin (Fig.1b), at a temperature too high for MSR (MSR is only efficient below 60°C; Machel et al., 1995; Machel, 2001), given that first hydrothermal arrivals in the borehole S9 occur at 261 m with a water temperature of 55.5 °C (Antea, 2009). On the contrary, TSR occurs at temperatures above 100 °C (Orr, 1977; Goldstein and Aizenshtat, 1994; Machel et al., 1995; Worden et al., 1995). This minimum temperature can be reached if waters supplying the caves migrate across or along Triassic evaporites through the faults in contact with the gneissic massif of Saint Barthélémy in the eastern part of the Tarascon-sur-Ariège basin (Fig.1b). Considering the high temperature measured in the S9 borehole, it is plausible that the geothermal gradient is abnormally high in this basin, with temperatures at depth reaching the condition for TSR, thereby producing H_2S in the more buried sedimentary series. High geothermal gradients up to 50°C/km have been recently identified in the Pyrenean Paleozoic Axial Zone and in the sedimentary cover close to the North Pyrenean Frontal Thrust (Bellahsen et al., 2019).

Proximity of the caves to the Pyrenean Axial Zone may thus explain a current high gradient.

To better constrain the role of TSR in H_2S production, and more particularly a partial reduction of Triassic evaporites in H_2S (coexistence of SO_4^{2-} and H_2S in the hydrothermal fluid), we built different mixing curves of MSI signatures between: (i) the Triassic evaporitic minerals at depth (sampled in the Arignac quarry) by considering dissolved SO_4^{2-} in ascending hydrothermal water, and (ii) the signatures of theoretic thermochemical H_2S poles which can be produced by TSR at respectively 100, 125 and 150°C (green and orange mixing interval in Fig.10) and also conveyed by the same hydrothermal fluid. MSI "mass-conservation effects" mixing curves between sulfur pools describe a convex hyperbolic $\Delta^{33}S$- $\delta^{34}S$ relationship (not a straight line) typical of a mixing between two sulfur pools according to the following equation (Farquhar et al., 2007):

$$\left(\frac{\delta^x S_{mix}}{1000}+1\right)=\left(\frac{\delta^x S_{TSR}}{1000}+1\right)\times \chi_{TSR}+\left(\frac{\delta^x S_{Triassic\ Evaporites}}{1000}+1\right)\times \chi_{Triassic\ Evaporites} \quad (3)$$

where x = 33 or 34, and χ_{TSR} and χ_{SO4} correspond to the fraction (between 0 and 1) of the TSR-derived H_2S and the Triassic evaporites respectively.

The $\Delta^{33}S$ value is then calculated using the equation (2). According to this calculation, mixing between two sulfur reservoirs thus leads to the generation of ^{33}S-depleted mixing products.

For the MSI signatures of TSR-derived H_2S, we calculated sulfur isotope fractionation values between Triassic sulfate minerals and the H_2S produced at 100, 125 and 150 °C by using fractionation equations between SO_4^{2-} and $H_2S_{(aq)}$ from Eldridge et al. (2016). For these calculations, it is assumed that the H_2S is generated at isotopic equilibrium from the initial Triassic sulfates and $HS_{(aq)}$. Fractionation calculations give three potential poles of pure TSR-derived H_2S: (i) $\delta^{34}S$ value of -27.04‰ and $\Delta^{33}S$ value of 0.027‰ at 100 °C, (ii) $\delta^{34}S$ value of -22.44‰ and $\Delta^{33}S$ value of 0.025‰ at 125 °C, and (iii) $\delta^{34}S$ value of -18.44‰ and $\Delta^{33}S$ value of 0.023‰ at 150 °C (Fig.10).

This method shows that the MSI signatures of two Ermite Cave gypsums (Erm2: $\delta^{34}S$ value of -5.06 ±0.01‰ V-CDT and $\Delta^{33}S$ value of -0.034 ±0.013‰; Erm3: $\delta^{34}S$ value of -7.33 ±0.008‰ V-CDT and $\Delta^{33}S$ value of -0.043 ±0.014‰) fall in the mixing trend between Triassic sulfate minerals and the TSR-derived H_2S poles, with a slightly more important relative contribution close to 55% of TSR-derived H_2S (Fig.10). Such MSI interpretations suggest that TSR is active today in the Northeastern Pyrenees, a fact not documented yet in the literature to our knowledge. The H_2S produced at great depth is subsequently conveyed through the anticline below Ussat-les-Bains by the hydrothermal water, along the faults and fractures affecting both Jurassic and Cretaceous carbonate formations to reach the studied caves (Fig.1b). This TSR-derived H_2S is mixed with unreduced SO_4^{2-} derived from leaching of Triassic evaporite formations at depth. As the ascending thermal fluid is poorly oxidizing (0.8 mg/l of dissolved oxygen against mean value of 8.07 mg/l in cave groundwater water close to the surface; Table 1), H_2S does not oxidize to sulfate before reaching the caves. Unfortunately, the lack of $\Delta^{33}S$ value of dissolved sulfate ions in cave sump waters does not allow us to constrain the origin of $\delta^{34}S$ values of +4.9 and +6.1 ±0.2‰ V-CDT, which is lower than Triassic evaporite signatures but higher than those of cave gypsum. It is likely that dissolved sulfate ions MSI signatures represent an intermediary state on the mixing curve in Figure 10, and potentially linked to the subsequent dissolution of gypsum during later cave evolution.

In addition, $\delta^{13}C$ value of degassing-derived calcites close to the thermal sump water in caves ($\delta^{13}C$ values of -7.3 ±0.2‰ V-PDB for calcite rafts in Vapeur Cave and -6.7/-6.6 ±0.2‰ V-PDB for folia in Ermite Cave) are lower than the host rock ($\delta^{13}C$ value of +0.3 ±0.2‰ V-PDB) (Fig.9a). It indicates either (i) biogenic carbon issued from CO_2 produced in overlying organic matter-rich soil, or (ii) thermochemical CO_2 (Palmer, 1991), as the TSR produces CO_2 during hydrocarbon oxidation (e.g. Hill, 1987; Machel, 2001). The evidence for active TSR inferred from MSI interpretation, and clear evidences of thermal water degassing (bubbles and abnormally high content of CO_2 in the cave atmosphere), indicate that at least a part of the CO_2 is of hydrothermal origin.

The MSI signature of one of the Ermite Cave gypsum sample (Erm1: $\delta^{34}S$ of -3.56 ±0.008‰ V-CDT and $\Delta^{33}S$ of -0.004 ±0.007‰) does not fall along the mixing trend between the Triassic evaporites and TSR-derived H_2S, but is much closer to the signatures of pyrites sampled in the Triassic evaporitic series in the Arignac underground quarry ($\delta^{34}S$ of +1.66 ±0.008 and +2.09 ±0.003‰ V-CDT, and $\Delta^{33}S$ of -0.003 ±0.008‰ and -0.010 ±0.010‰, respectively) (Fig.10). This could indicate that the leaching of pyrite veins, only reported in Triassic series at depth, can be a

supplementary source of sulfur to the caves. Abiotic oxidation of sulfides may induce a small $\delta^{34}S$ fractionation up to 5‰ (Fry et al., 1988; Findlay et al., 2019), which can be compatible with the signature of the cave gypsum Erm1. A thermodynamic model was performed using the PhreeqC software (Parkhurst and Appelo, 1999) and using the SUPCRT92 database (Johnson et al., 1992), to determine the concentration of sulfides released during pyrite oxidation between 25 and 200 °C. The fluid composition of the thermo-mineral water from S9 borehole (Antea, 2009) was used in equilibrium with excess of pyrite and heated between 25 and 200 °C. This model shows that the more the temperature increases, the more H_2S is released. Dissolved sulfide concentration is significant at 150 °C with 3×10^{-3} mmol/kg_{H2O} and rises to 4×10^{-2} mmol/kg_{H2O} at 200 °C. As iron is necessarily released during the hydrothermal leaching of pyrites, iron can precipitate at 150 °C as hematite and goethite (e.g. Collon et al., 2006), which would explain its absence in the hydrothermal fluids (Table 1). In addition, former air pockets in caves are coated by iron- and manganese-rich incrustations (Fig.7a), which suggest that iron can also be present in the cave and could derived from: (i) the alteration of silicate rocks from glacial karstic sediments stored in the shaft, and (ii) Fe^{2+} from pyrite alteration conveyed by hydrothermal fluids up to the caves and deposited early during mixing with meteoric infiltrations at water-air interface. These small amounts of H_2S released by pyrite leaching can thus be added to the TSR-derived H_2S and Triassic sulfate mixing in the hydrothermal water that reached the karstic network to form the sulfuric acid in the oxidizing cave atmosphere.

Sulfate-carbonate substitution front inferred from $\delta^{34}S$ values of trace sulfate minerals

In hypogenic sulfuric caves, reactions between sulfuric acid and calcium, the latter being released during sulfuric acid dissolution of the host carbonate rock, are responsible for the precipitation of gypsum in replacement of the host rock (e.g. Egemeier, 1981, 1987; Galdenzi and Maruoka, 2003). The sulfate-carbonate substitution rate is higher than the invasion rate of sulfuric acid and consequently does not allow the development of thick alteration zones. It is thus commonly assumed that the sulfate-substitution front, if present, is only 1 mm-thick (Plan et al., 2012). However, the negative values of $\delta^{34}S$ of trace sulfates in the host carbonate rock of the Ermite Cave, up to c.a. 1 cm from the gypsum-carbonate interface, indicate the invasion of substitution sulfates and thus a more developed substitution front than those described in previous studies (Fig.11). This substitution is only possible in the case of SAS, confirming the hypogenic influence associated with the gypsum formation. The gradual increase of $\delta^{34}S$ values from gypsum values to those of the unaltered carbonate (from -9.5 to +9.3 ±0.2‰ V-CDT) is here attributed to a buffering effect of the sulfur isotopic signatures of replacement sulfate minerals by the CAS (carbonate-associated sulfates) of the host rock during the progressive invasion of sulfuric acid and associated carbonate dissolution. Analyses of trace sulfate minerals present in the cave host rock thus represent a proxy to identify the action of hypogenic sulfuric acid dissolution if replacement gypsum has been removed by subsequent leaching.

5.3. Epigenic vs. hypogenic karstification during glacial/interglacial periods

Analyses of cave morphologies and sedimentary fillings reveal that the studied karstic networks can be subdivided into two distinct parts: (i) an upper horizontal part having recorded a former base-level and significant meltwater glacier flow marks, without notable evidence of hypogenic influence; and (ii) an underlying sub-vertical shaft which corresponds to a typical *per ascensum* "feeder", at least partially formed by carbonic and sulfuric condensation-corrosion during a more pronounced hypogenic component linked to the degassing of a hydrothermal water table.

However, various morphological and mineral markers observable today are inherited from a recent phase of the cave evolution, and are most certainly related to the last glacial/interglacial cycle (last glacier retreat in the valley between 19 and 18 ka; Delmas et al., 2012). This partial destruction of ancient evolution marks limits the interpretation of the cave genesis. The dating of cave sediments and speleothems carried out in nearby Niaux-Lombrives-Sabart karstic systems (other side of the same Ariège Valley) revealed that several rejuvenations of the karsts by subterranean epigenic invasions took place during all the glacial/interglacial successions occurring during the last 450 kyr (Sorriaux et al., 2016), but also highlighted epigenic events as early as c.a. 8 Myr ago (Sartégou et al., 2020). This 8 Ma date therefore confirms that the genesis of karsts along the Ariège Valley was initiated during the Late Miocene or even before, and the evolution was certainly continuous from that time.

Significant hydrothermal circulations in the Eastern Pyrenees took place during two extensional phases linked to the opening of the Gulf of Lion, with the

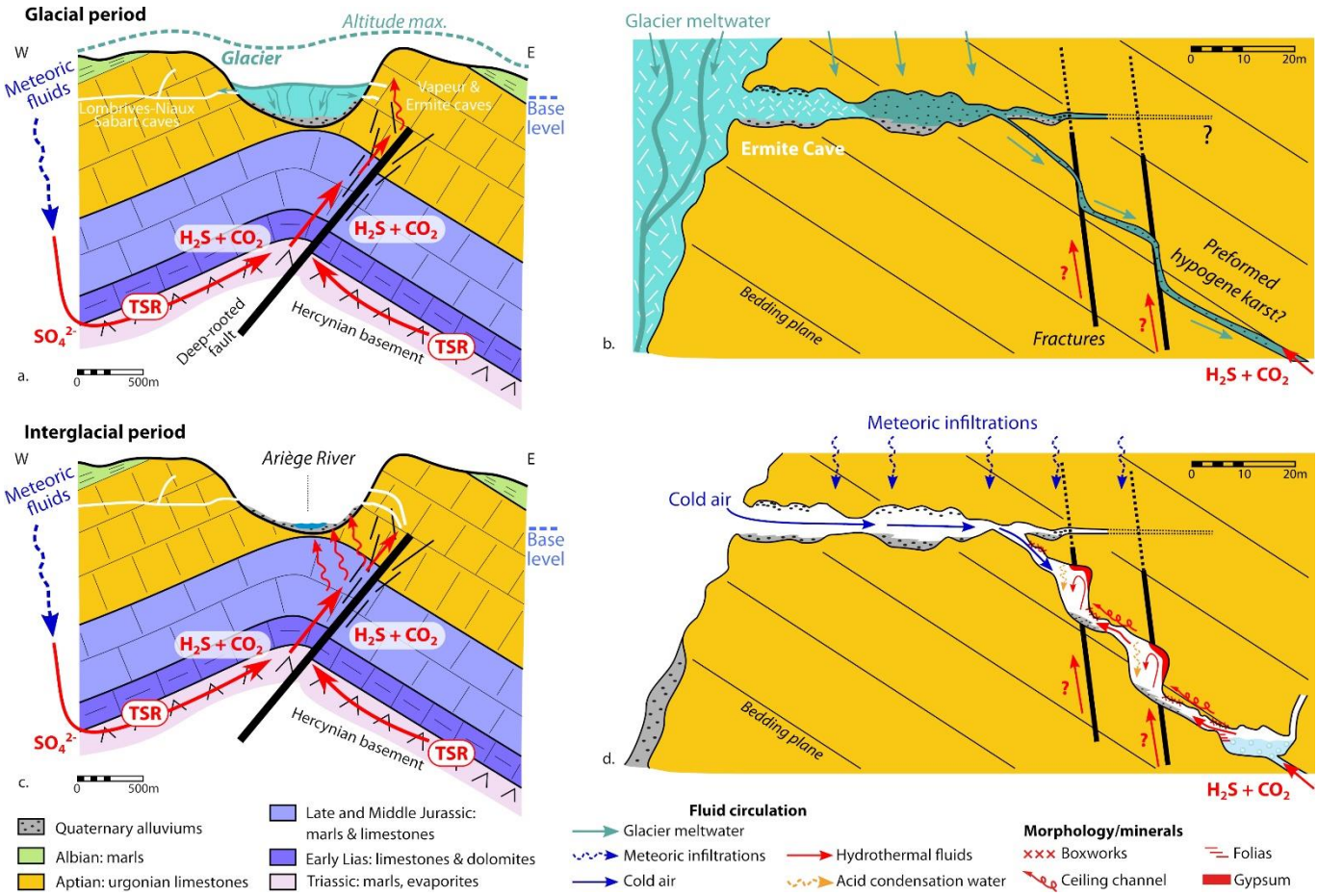

Figure 12: Speleogenetic model in the Ermite and Vapeur caves during Quaternary glacial/interglacial cycles alternations. a. and b. *"Epigenic mechanical-dominant"* karstification: ice- and meltwater-related abrasion when the Ariège valley was covered by icefield in glacial periods (regional scale (a) and cave scale (b)). Meltwater invasion led to the weakening of hydrothermal input influence in caves through dilution process and plugging by cave sediments in the lower shaft. c. and d. *"Hypogenic chemical-dominant"* speleogenesis following the base-level drop during interglacial epoch: vadose domain favored the impact of thermochemical CO_2- and H_2S-rich hydrothermal fluids on karstification, linked to carbonic and sulfuric acid condensation-corrosion in the cave atmosphere generated by warm sump water degassing.

activation and reactivation of NW-SE and NE-SW trending faults occurring from the Early Oligocene to the Early Miocene, and from the Early Miocene to the Late Pliocene (e.g. Séranne, 1999). The tectonic activity of these faults was associated with the onset of hydrothermalism in the Pyrenean Axial Zone (e.g. Taillefer et al., 2017) and could also be at the origin of the thermal activity in the Ariège Valley. Consequently, even in the absence of intact morphological markers, a plausible hypothesis is that the initiation phase of both Vapeur and Ermite caves would correspond to the development of hypogene sub-vertical feeders, possibly during the Miocene, resulting from hydrothermal upwelling through fractures and bedding planes. It is therefore only in later phases that the sub-vertical parts of the caves were intersected and rejuvenated by sub-horizontal epigenic galleries connected to a former Ariège valley base-level higher than today, and linked to glacial meltwater circulations during Quaternary glacial/interglacial periods.

The discussion in the next sections will be based on the interpretation of morphologies and minerals visible today, and consequently only focuses on the evolution of the Vapeur and Ermite caves during the last glacial/interglacial cycle. Analysis of the last climatic cycle provides a speleogenetic model in which two distinct processes alternated, depending on the intensity of the meteoric component during a constant hydrothermal circulation: (i) an *"epigenic mechanical-dominant"* karstification during glacial periods, and (ii) a *"hypogenic chemical-dominant"* speleogenesis during interglacial epochs and still active today.

"Epigenic mechanical-dominant" karstification during glacial periods

During Quaternary glacial periods, hydrological base-level of the Ariège Valley was higher than today, controlled by the icefield dynamics (Delmas et al., 2012). Consequently, pre-existing karstic networks on both sides of the valley (Lombrives-Niaux-Sabart and Vapeur-Ermite caves) were affected by flooding torrents of glacier meltwater, more particularly during cataglacial phases (Sorriaux et al., 2016) (Fig.12a), and were locally invaded by short subterranean ice tongues near cave entrances (Fig.12b). During glacier advance, the increase of hydraulic gradients through higher pressure and water supply can enlarge active galleries through subterranean abrasion (Lauritzen, 2006). In the upper galleries of both the Ermite and Vapeur caves, meltwater conveyed clastic particles, as confirmed by relics of coarse clastic infillings and intense polishing of some cave walls (Fig.5). The polishing process was likely related to rapid movements of sand particles inducing wall abrasion during water invasion with high hydraulic head, as expected during seasonally hydraulic changes within moving ice tongues. Geometry of scallops in the Ermite Cave, slightly carving the cave wall, shows an overall NE-SW-oriented flow, indicating that the current entrances of the cave represented the outlet of meltwater invasions towards the Ariège Valley (but the former entrance in the NE remains unexplored). The surface water (rainfall, ice and snow meltwaters) circulating into the karst was probably weakly acid because of poorly vegetated soils. This process thus disadvantaged limestone dissolution and speleothem precipitation (e.g. Audra et al., 2007b) and both Ermite and Vapeur cave probably only slightly enlarged by dissolution during these epochs. At this time, only horizontal conduits were active as cave sediments progressively entirely plugged the underlying sub-vertical feeder located at depth below the water table (as observed on relics of cave sediments on the ceiling; Fig.4b), and thus representing a sub-horizontal by-pass for water toward the valley (Fig.12b). In addition, fine fluvioglacial sediments in the upper galleries can even more protect the cave wall from chemical weathering (e.g. Audra et al., 2007b). A high surface water supply implied that the hydrothermal flow, which probably still rose up from the bottom of the drowned Ermite and Vapeur caves (as observed today), was strongly diluted with meltwater inputs. This complete filling by cave sediments therefore decreased the influence of hypogenic CO_2 and H_2S inputs on the karstic processes, probably limited only to ceiling channels at the interface between karstic sediments and cave ceiling (Fig.12b).

"Hypogenic chemical-dominant" karstification during interglacial periods

Retreat of glaciers at the beginning of the interglacial period inevitably led to a modification of hydrological regime in both Ermite and Vapeur caves, their upper parts becoming perched several tens of meters above the base-level, and consecutively abandoned by water flows (Fig.12c). In the upper phreatic zone and in the lower vadose zone, the low flux of warm water and gas rising at cave terminal sumps (0.7 to 1.4% of CO_2 in the Ermite Cave atmosphere) played an important role in speleogenesis, particularly through sulfuric and carbonic acid speleogenesis (Fig.12d). In such hypogenic conditions, CO_2 and H_2S degassing and hydration/oxidation is most efficient at or immediately above the water surface (De Waele et al., 2016; D'Angeli et al., 2019), meaning that such caves are reliable indicators of past water table levels and can help in determining base-level changes over time (Piccini et al., 2015; De Waele et al., 2016). Above the water table, various corrosion features and minerals (ceiling channels, ceiling cupolas, aerial convection niches, corrosion furrows and karren, popcorn-like calcite, folia, calcite rafts) confirm that the most significant karstification process was linked to a thermal condensation-corrosion associated to a vadose domain during thermo-mineral water degassing. Precipitated in these hypogene morphologies, calcite and substitution gypsum in the host carbonate rocks show typical carbon and multiple sulfur isotopic composition of carbonic and sulfuric karstification (*i.e.* negative values for $\delta^{13}C$ of related calcites (Fig.9a) and for $\delta^{33}S$ and $\delta^{34}S$ of sulfate minerals; Fig.10 and 11), which confirm the link between dissolution features and neoformed minerals/alteration linked to the action of carbonic and sulfuric acids. As only a small amount of cave sediments is still preserved on the cave floor and ceiling, and intensively corroded (Fig.7e), it indicates a subsequent complete erosion of sedimentary infilling that previously obstructed this part of the cave. Cave sediments were probably first weathered in phreatic conditions before the complete retreat of the glacier, and was followed by a partial dissolution and destabilization through sub-aerial condensation-corrosion in vadose conditions that dissolved the carbonate part (15 to 20%) and led to the hydrolyze of the clay fraction (e.g. Audra et al., 2016). Then, the sandy residual sediments (not easily altered by condensation-corrosion) could be evacuated by

sudden hydraulic purge during late melting phases of perched residual glaciers, either directly to the cave outlet toward the Ariège Valley or to the base of the caves, thus clogging a part of the sump. In the Lombrives-Niaux-Sabart karstic networks, located on the other side of the same valley, an almost complete cave sediment removal took place during MIS4 and MIS2 (Würm; Sorriaux et al., 2016), which gives the timing of cessation of significant surface water input, and thus can correspond to the peak of the hydrothermal influence in both Vapeur and Ermite caves.

Nowadays, before reaching the cave sumps, CO_2- and H_2S-rich hydrothermal fluids leach Triassic evaporite formations before migrating along fractures structuring the faulted anticline below the studied caves (Fig.12c). Hypogenic fluids also reach and diffuse within fluvio-glacial alluviums of the Ariège valley feeding several warm springs. In the lower parts of Ermite and Vapeur caves, several observations demonstrate that the influence of CO_2 and H_2S inputs was not constant, with alternation of periods of precipitation and dissolution of calcite and/or gypsum. Indeed, if the current absence of H_2S in the cave atmosphere (during our field investigations) is probably linked to its fast oxidation into sulfuric acid and gypsum, and dilution by air flow entering the cave in cold days, texture analyses of cave gypsum highlight different steps of dissolution-reprecipitation processes (needles and blisters vs. saccharoidal crusts; Fig.8c and 8d). Textures of dissolution-reprecipitation of cave gypsum can be associated with either a lower H_2S content in the cave atmosphere at a specific time, or an increase of CO_2 degassing which enhanced the carbonic condensation-corrosion on the cave wall. Hypogenic carbonic speleogenesis and strong condensation can be the reason for the lack of gypsum in the unsheltered areas of the Ermite Cave and its complete absence from the Vapeur Cave, in addition to a slight dissolution by discrete meteoric infiltrations. Confirming the variable CO_2 degassing, cave walls exhibit several generations of calcite coatings, some of them affected by corrosion furrows while more recent ones covered these dissolution features (Fig.7c). Periodic CO_2 and H_2S content in caves can also be associated with local climate variations that induced changes in the intensity of airflow convection in the cave atmosphere. Indeed, CO_2 concentration in the Ermite Cave atmosphere is twice that in summer (1.4%) respect to that in winter (0.7%). During the winter, cold air sinks into the deepest part of the karstic networks and induces the dilution of gas in the cave atmosphere, which explains the lower CO_2 concentration. On the contrary, during summer periods, warm air from the cave sump rises toward the surface and is not diluted. Higher magnitudes of climate changes during interglacial and deglaciation periods was probably responsible for larger variations of CO_2 and H_2S contents during the whole history of caves. In addition to climate impact, the periodic inputs of deep CO_2 and H_2S can be also attributed to potential hydrothermal pulses during tectonic reactivation of deep faults structuring the anticline (Fig.12c) (earthquakes and fluid overpressure such as seismic valve process; e.g. Sibson, 1992; Laurent et al., 2017).

As previously mentioned, our climate-driven speleogenetic model describes the recent evolution of the karstic networks since the Würm glaciation. However, as the genesis of these caves would started during the Miocene, same scenarios could have taken place during all Quaternary glacial/interglacial cycles. In this case, the *"hypogenic chemical-dominant speleogenesis"* was dominant until icefields cover the valley again, reactivating karstic systems through glacier tongues and meltwater invasion. These invasions indeed weakened the hypogenic influence and, possibly, even displaced upward this hypogenic influence toward more elevated and unknown non-flooded parts of the karstic networks located along the valley flank.

6. Conclusions and perspectives

This study proposes an integrated method combining the geomorphological analysis of two partially hypogenic caves in the Ariège Valley (Ermite and Vapeur caves), the mineralogy and texture of specific cave minerals (calcite and sulfate minerals), together with geochemistry and various isotope studies (S, C, Sr, O, H) of thermo-mineral waters and cave minerals. From this methodology, a multi-phase history of alternating epigenic and hypogenic speleogenesis phases was identified. These events were driven by climate changes related to Quaternary glacial/interglacial periods in the valley.

Several points can be retained from this study:

- Deciphering epigenic from hypogenic speleogenesis requires the identification of hydrothermal fluid nature and migration pathways at both regional and cave scales. In this objective, multiple sulfur isotopy (MSI) appears necessary to really constrain the nature and mixing of sulfur-rich fluids and the

potential role of Sulfuric Acid Speleogenesis (SAS). In particular, we prove the relevance of mixing curves in a $\Delta^{33}S$ vs. $\delta^{34}S$ diagram to identify the different poles of sulfur implied in the hypogenic speleogenesis. In addition to SAS evidences, this method allows, for the first time in the Pyrenees, the identification of currently active Thermochemical Sulfate Reduction (TSR) of the Triassic evaporites at depth;

- In such a karstic region concerned by a perennial hydrothermal activity, the respective impact of epigenic and hypogenic speleogenesis is controlled by the base-level changes during glacier advance/retreat dynamics (phreatic vs. vadose domain in caves), and the degree of meltwater invasion in the karst. Two superimposed speleogenetic processes during karst history are highlighted here: (i) *"epigenic mechanical-dominant"* speleogenesis during glacial periods, linked to the penetration of torrential glacial meltwater in caves and to the dilution of ascending hydrothermal water; and (ii) a *"hypogenic chemical-dominant"* karstification in vadose domain, during an interglacial base-level drop, associated with sulfuric and carbonic acid condensation-corrosion above the thermal water table (inferred from the association between typical cave condensation-corrosion morphologies, negative $\delta^{13}C$ values of related calcites, and negative $\delta^{33}S$ and $\delta^{34}S$ values of gypsum occurring in substitution of the host rock). Condensation-corrosion were able, not only to enlarge cave passages by acidic solution, but also to partially remove the previous fluvio-glacial infilling of conduits;

- Hypogenic cave atmosphere can be characterized by unstable conditions due to climate changes (that modify the airflow circulation in the caves). Moreover, seismic-controlled sudden and unpredictable hydrothermal H_2S and CO_2-rich pulses might also have occurred. Consequently, such caves constitute preferential seep areas for dangerous gas emissions for speleologists (Ermite and Vapeur caves are often used for visits). For instance, high level of H_2S (commonly > 150 ppm) cannot be smelled but can be fatal. Thus, in order to better understand their atmospheric dynamics and to prevent accidents, it would be relevant to monitor the gas concentration in such hydrothermal cavities.

Acknowledgments

This work was financially supported by TOTAL EP R&D (Pau, France, Project Leader Sylvain Calassou) at CREGU. This study has benefited from discussions with Didier Cailhol (INRAP/Edytem, France) and Jean-Yves Bigot (Association Française de Karstologie; which also provides one photo used in this article). We are grateful to Danièle Bartier and Odile Barres for their technical support with XRD and DRIFT analyses respectively at GeoRessources lab (Nancy, France). We thank Sidonie Revillon for strontium isotope measurements on sulfate minerals at IUEM (Plouzané, France), Nadège Lagasse, Julie Marquis and Carole Bortelle for oxygen isotope analysis at Scientific and Technical Centers of the Universitat de Barcelona (Spain), and BRGM lab (France) for physico-chemical analysis and oxygen, hydrogen and strontium isotope measurements of thermo-mineral waters. Robert Guinot and the SCHS speleological club are greatly thanked for their support during the several exploration phases of numerous caves along the Ariège Valley. Finally, the Editor Achim A. Beylich and the two reviewers, Jo De Waele and Augusto Auler, are thanked for thoughtful and constructive reviews which greatly improved the manuscript.

References

Antea, 2009. Forage d'eau minérale S9 à Ornolac- Ussat-les-Bains (09). Dossier de déclaration au titre de l'article 214.1 et suivants du Code de l'Environnement, 92p.

Assayag N., Jézéquel D., Ader M., Viollier E., Michard G., Prévot F., Agrinier P., 2008. Hydrological budget, carbon sources and biogeochemical processes in Lac Pavin (France): constraints from $\delta^{18}O$ of water and $\delta^{13}C$ of dissolved inorganic carbon. Appl. Geochem. 23(10), 2800-2816.

Audra P., 2007. Karst et spéléogenèse épigènes, hypogènes, recherches appliquées et valorisation. Habilitation Thesis, University of Nice Sophia-Antipolis, 278 p.

Audra P., 2017. Hypogenic Caves in France. In: Klimchouk A., N. Palmer A., De Waele J., S. Auler A., Audra P. (eds) hypogene Karst Regions and Caves of the World. Cave and Karst Systems of the World. Springer, 61-83.

Audra, P., Hoblea, F., Bigot, J. Y., Nobecort, J. C., 2007a. The Role of Condensation Corrosion in Thermal Speleogenesis. Study of a Hypogenic Sulfidic Cave in Aix-les-Bains, France. Acta carsologica, 36(2).

Audra, P., Bini, A., Gabrovšek, F., Häuselmann, P., Hobléa, F., Jeannin, P. Y., Kunaver, J., Monbrano, M., Sustersic, F., Tognini, P., Trimmel, H., Wildberger, A., 2007b. Cave

and karst evolution in the Alps and their relation to paleoclimate and paleotopography. Acta carsologica, 36(1).

Audra, P., Mocochain, L., Bigot, J.Y., Nobécourt, J.C., 2009. The association between bubble trails and folia: a morphological and sedimentary indicator of hypogenic speleogenesis by degassing, example from Adaouste Cave (Provence, France). International Journal of Speleology, 38(2), 93-102.

Audra, P., Barriquand, L., Bigot, J. Y., Cailhol, D., Caillaud, H., Vanara, N., Nobecourt, J. C., Madonia, G., Vattano, M., Renda, M, 2016. L'impact méconnu des chauves-souris et du guano dans l'évolution morphologique tardive des cavernes. Karstologia, 68.

Bakalowicz, M., Sorriaux, P., Ford, D.C., 1984. Quaternary glacial events in the Pyrenees from U–series dating of speleothems in the Niaux– Lombrives–Sabart caves, Ariège, France. Norsk Geografisk Tidsskrift, 38, 193-197.

Bellahsen, N., Bayet, L., Denele, Y., Waldner, M., Airaghi, L., Rosenberg, C., Dubacq, B., Mouthereau, F., Bernet, M., Pik, R., Lahfid, A., Lahfid, A., 2019. Shortening of the axial zone, pyrenees: Shortening sequence, upper crustal mylonites and crustal strength. Tectonophysics, 766, 433-452.

Biteau, J. J., Le Marrec, A., Le Vot, M., Masset, J. M., 2006. The aquitaine basin. Petroleum Geoscience, 12(3), 247-273.

BRGM, 1983. Report code 1087 3X 0012, in database "Banque du Sous-Sol BSS".

Cai, C., Worden, R. H., Bottrell, S. H., Wang, L., Yang, C., 2003. Thermochemical sulphate reduction and the generation of hydrogen sulphide and thiols (mercaptans) in Triassic carbonate reservoirs from the Sichuan Basin, China. Chemical Geology, 202(1-2), 39-57.

Calvet M., 1996. Morphogenèse d'une montagne méditerranéenne, les Pyrénées-Orientales, Document du BRGM 255, Orléans, 3 t., pochette de cartes hors texte, 1177p.

Canfield, D. E., Raiswell, R., Westrich, J. T., Reaves, C. M., Berner, R. A., 1986. The use of chromium reduction in the analysis of reduced inorganic sulfur in sediments and shales. Chemical geology, 54(1-2), 149-155.

Cigna, A. A., Forti, P., 1986. The speleogenetic role of air flow caused by convection. 1st contribution. International Journal of Speleology, 15(1), 41-52.

Collon, P., Fabriol, R., Buès, M., 2006. Modelling the evolution of water quality in abandoned mines of the Lorraine Iron Basin. Journal of hydrology, 328(3-4), 620-634.

Columbu, A., Audra, P., Gázquez, F., D'Angeli, I. M., Bigot, J. Y., Koltai, G., Chiesa, R., Yu, T-L., Hu, H-M., Shen, C-C., Carbone, C., Heresanu, V., Nobécourt, J-C., De Waele, J, 2021. Hypogenic speleogenesis, late stage epigenic overprinting and condensation-corrosion in a complex cave system in relation to landscape evolution (Toirano, Liguria, Italy). Geomorphology, 376, 107561.

Connan, J., Lacrampe-Couloume, G., 1993. The origin of the Lacq superieur heavy oil accumulation and the giant Lacq inferieur gas field. Applied Petroleum Geochemistry, 3, 464-488.

Craig, H., 1961. Isotopic variations in meteoric waters. Science, 133(3465), 1702-1703.

D'Angeli, I.M., De Waele, J., Ceballo Melendres, O., Tisato, N., Sauro, F., Grau, González, E.R., Bernasconi, S.M., Torriani, S., Bontognali. T.R.R., 2015. Genesis of folia in a non-thermal epigenic cave (Matanzas, Cuba). Geomorphology, 228, 526–535.

D'Angeli, I. M., Nagostinis, M., Carbone, C., Bernasconi, S. M., Polyak, V. J., Peters, L., McIntosh, W. C., De Waele, J., 2019. Sulfuric acid speleogenesis in the Majella Massif (Abruzzo, Central Apennines, Italy). Geomorphology, 333, 167-179.

Delmas, M., Calvet, M., Gunnell, Y., Braucher, R., Bourles, D., 2011. Palaeogeography and 10Be exposure-age chronology of Middle and Late Pleistocene glacier systems in the northern Pyrenees: implications for reconstructing regional palaeoclimates. Palaeogeography, Palaeoclimatology, Palaeoecology, 305(1-4), 109-122.

Delmas, M., Calvet, M., Gunnell, Y., Braucher, R., Bourlès, D., 2012. Les glaciations quaternaires dans les Pyrénées ariègeoises: approche historiographique, données paléogéographiques et chronologiques nouvelles. Quaternaire. Revue de l'Association française pour l'étude du Quaternaire, 23(1), 61-85.

De Waele, J., Audra, P., Madonia, G., Vattano, M., Plan, L., D'Angeli, I. M., Bigot, J.-Y, Nobécourt, J.-C., 2016. Sulfuric acid speleogenesis (SAS) close to the water table: examples from southern France, Austria, and Sicily. Geomorphology, 253, 452-467.

Dreybrodt, W., Gabrovšek, F., Perne, M., 2005. Condensation corrosion: a theoretical approach. Acta Carsologica, 34(2).

Dublyansky, Y. V., Pashenko, S. E., 1997. Cave popcorn: an aerosol speleothem. In 12th International Congress of Speleology, Swiss Speleological Society, Proceedings, Vol. 1, 271-274.

Dublyansky, V. N., Dublyansky, Y. V., 2000. 3.6. Role of condensation in Karst hydrogeology and speleogenesis. Speleogenesis: Evolution of Karst aquifers. Eds. AB Klimchouk, DC Ford, AN Palmer, W. Dreybrodt. Huntsville, Alabama, USA. National Speleological Society, 100-112.

Dublyansky Y.V., 2000. Hydrothermal speleogenesis – its settings and peculiar features. In: Klimchouk A., Ford D.C., Palmer A.N., Dreybrodt W., (Eds). Speleogenesis: evolution of karst aquifers. Huntsville: National Speleological Society, 292-297.

Dublyansky, Y., Spötl, C., 2009. Identifying paleo water-rock interaction during hydrothermal karstification: a stable isotope approach. Hypogene Speleogenesis and Karst Hydrogeology of Artesian Basins, Ukrainian Institute of Speleology and Karstology Special Paper, 1.

Dublyansky, Y.V., Klimchouk, A. B., Spötl, C., Timokhina, E. I., Amelichev, G. N., 2014. Isotope wallrock alteration associated with hypogene karst of the Crimean Piedmont, Ukraine. Chemical Geology 377, 31-44.

Dublyansky, Y. V., Spötl, C., 2014. Morphological effects of condensation-corrosion speleogenesis at Devils hole ridge, Nevada. Hypogene Cave Morphologies, Karst Waters Institute special publication 18, 36-43.

Eldridge, D. L., Guo, W., Farquhar, J., 2016. Theoretical estimates of equilibrium sulfur isotope effects in aqueous sulfur systems: Highlighting the role of isomers in the sulfite and sulfoxylate systems. Geochimica et Cosmochimica Acta, 195, 171-200.

Egemeier, S. J., 1981. Cavern development by thermal waters. NSS Bulletin, Volume 43 (2), 31-51.

Egemeier, S. J., 1987. A theory for the origin of Carlsbad Caverns. NSS Bulletin 49 (2), 73-76.

Farquhar, J., Johnston, D. T., Wing, B. A., Habicht, K. S., Canfield, D. E., Airieau, S., Thiemens, M. H., 2003. Multiple sulphur isotopic interpretations of biosynthetic pathways: implications for biological signatures in the sulphur isotope record. Geobiology, 1(1), 27-36.

Farquhar, J., Johnston, D. T. Wing, B. A, 2007. Implications of conservation of mass effects on mass-dependent isotope fractionations: Influence of network structure on sulfur isotope phase space of dissimilatory sulfate reduction. Geochimica et Cosmochimica Acta, 71(24), 5862-5875.

Findlay, A. J., Boyko, V., Pellerin, A., Avetisyan, K., Guo, Q., Yang, X., Kamyshny Jr, A. 2019. Sulfide oxidation affects the preservation of sulfur isotope signals. Geology, 47(8), 739-743.

Ford, D., Williams, P.W., 2007. Karst hydrogeology and geomorphology. John Wiley & Sons, 576p.

Forti, P., Sanna, L., 2010. The Naica Project-A multidisciplinary study of the largest gypsum crystals of the world. Episodes, 33(1), 23-32.

Fry, B., Ruf, W., Gest, H., Hayes, J. M. 1988. Sulfur isotope effects associated with oxidation of sulfide by O_2 in aqueous solution. Chemical Geology: Isotope Geoscience section, 73(3), 205-210.

Galdenzi, S., Maruoka, T., 2003. Gypsum deposits in the Frasassi Caves, central Italy. Journal of Cave and Karst Studies, 65(2), 111-125.

Goldscheider, N., Chen, Z., Auler, A. S., Bakalowicz, M., Broda, S., Drew, D., Hartmann, J., Jiang, G., Moosdorf, N., Stevanovic, Z., Veni, G., 2020. Global distribution of carbonate rocks and karst water resources. Hydrogeology Journal, 28(5), 1661-1677.

Goldstein, T., Aizenshtat, Z., 1994. Thermochemical sulfate reduction a review. Journal of Thermal Analysis and Calorimetry, 42(1), 241-290.

Heydari, E., Moore, C. H., 1989. Burial diagenesis and thermochemical sulfate reduction, Smackover Formation, southeastern Mississippi salt basin. Geology, 17(12), 1080-1084.

Hill, C. A., 1987. Geology of Carlsbad cavern and other caves in the Guadalupe Mountains, New Mexico and Texas. Bull. 117, New Mexico Bureau of Mines and Minerals Resources (USA), 161p.

Hill, C. A., Forti, P., 1997. Cave minerals of the world: Huntsville. Alabama, National Speleological Society, 285-287.

Hill, C. A., Polyak, V. J., 2010. Karst hydrology of Grand Canyon, Arizona, USA. Journal of Hydrology, 390(3-4), 169-181.

Horibe, Y., Shigehara, K., Takakuwa, Y., 1973. Isotope separation factor of carbon dioxide-water system and isotopic composition of atmospheric oxygen. Journal of Geophysical Research, 78(15), 2625-2629.

Johnston, D. T., Farquhar, J., Canfield, D. E., 2007. Sulfur isotope insights into microbial sulfate reduction: when microbes meet models. Geochimica et Cosmochimica Acta, 71(16), 3929-3947.

Johnston, D. T., 2011. Multiple sulfur isotopes and the evolution of Earth's surface sulfur cycle. Earth-Science Reviews, 106(1-2), 161-183.

Johnson, J.W., Oelkers, E.H., Helgeson, H.C., 1992. SUPCRT92: A software package for calculating the standard molal thermodynamic properties of minerals, gases, aqueous species, and reactions from 1 to 5000 bar and 0 to 1000 C. Computers & Geosciences, 18(7), 899-947.

Kitayama, Y., Thomassot, E., Galy, A., Golovin, A., Korsakov, A., d'Eyrames, E., Assayag, N., Bouden, N., Ionov, D., 2017. Co-magmatic sulfides and sulfates in the Udachnaya-East pipe (Siberia): A record of the redox state and isotopic composition of sulfur in kimberlites and their mantle sources. Chemical Geology, 455, 315-330.

Klanica, R., Kadlec, J., Tábořík, P., Mrlina, J., Valenta, J., Kováčiková, S., Hill, G. J., 2020. Hypogenic Versus Epigenic Origin of Deep Underwater Caves Illustrated by the Hranice Abyss (Czech Republic) —The World's Deepest Freshwater Cave. Journal of Geophysical Research: Earth Surface, 125(9), e2020JF005663.

Klimchouk, A. B., 2007. Hypogene speleogenesis: hydrogeological and morphogenetic perspective. National Cave and Karst Research Inst., Carlsbad, United States, 106p.

Klimchouk, A., Sasowsky, I. D., Mylroie, J., Engel, S. A., Engel, A. S., 2014. Hypogene cave morphologies. Selected papers and abstracts of the symposium held February 2 through 7, San Salvador Island, Bahamas. Karst Waters Institute Special Publication 18, Karst Waters Institute, Leesburg, Virginia. 111 p.

Klimchouk, A., Palmer, A. N., De Waele, J., Auler, A. S., Audra, P. (Eds.), 2017. Hypogene karst regions and caves of the world. Springer, 911p.

Koepnick, R.B., Denison, R.E., Burke, W.H., Hetherington, E.A., Dahl, D.A., 1990. Construction of the triassic and Jurassic portion of the Phanerozoic curve of seawater $^{87}Sr/^{86}Sr$. Chem. Geol. Isot. Geosci. Sect. 80, 327–349.

Laurent, D., Lopez, M., Chauvet, A., Sauvage, A.C., Buatier, M., Spangenberg, J.E., 2017. Sedimentary fluids/fault interaction during syn-rift burial of the Lodève Permian Basin (Hérault, France): an example of seismic-valve mechanism in active extensional faults. Mar. Petrol. Geol. 88, 303–328.

Lauritzen, S. E., 2006. Caves and speleogenesis at Blomstrandsøya, Kongsfjord, W. Spitsbergen. International Journal of Speleology, 35(1), 37-58.

Leél-Őssy, S., 2017. Caves of the Buda Thermal karst. In Hypogene Karst Regions and Caves of the World (eds. A.B. Klimchouk, A.N. Palmer, J. De Waele, A.S. Auler, A. S. and P. Audra), 279-297.

López-Martínez, R., Gázquez, F., Calaforra, J. M., Audra, P., Bigot, J. Y., Pi Puig, T., Alcántara-Hernández, R. J., Navarro, Á., Crochet, P., Martinez, L. C., Brunet, R. D., 2020. Bubble trail and folia in cenote Zapote, Mexico: petrographic evidence for abiotic precipitation driven by CO_2 degassing below the water table. International Journal of Speleology, 49(3), 173-186.

Machel, H. G., Krouse, H. R., Sassen, R., 1995. Products and distinguishing criteria of bacterial and thermochemical sulfate reduction. Applied geochemistry, 10(4), 373-389.

Machel, H. G., 2001. Bacterial and thermochemical sulfate reduction in diagenetic settings—old and new insights. Sedimentary Geology, 140(1-2), 143-175.

Monod, B., Regard, V., Carcone, J., Wyns, R., Christophoul, F., 2016. Postorogenic planar paleosurfaces of the central Pyrenees: weathering and neotectonic records. Comptes Rendus Géoscience, 348 (3-4), pp.184-193.

Mylroie, J. E., Carew, J. J., 1988. Solution conduits as indicators of late Quaternary sea level position. Quaternary Science Reviews, 7(1), 55-64.

Mylroie, J. R., Mylroie, J. E., 2007. Development of the carbonate island karst model. Journal of Cave and Karst Studies, 69(1), 59-75.

Onac, B. P., Wynn, J. G., Sumrall, J. B., 2011. Tracing the sources of cave sulfates: a unique case from Cerna Valley, Romania. Chemical Geology, 288(3-4), 105-114.

Orr W. L., 1977. Geologic and geochemical controls on the distribution of hydrogen sulfide in natural gas. In: Campos R and Goni J (eds.). Advances in organic geochemistry. Enadimsa, Madrid Spanish, 571-597.

Palmer, A. N., 1991. Origin and morphology of limestone caves. Geological Society of America Bulletin, 103(1), 1-21.

Palmer, A. N., Palmer, M. V., 2000. Hydrochemical interpretation of cave patterns in the Guadalupe Mountains, New Mexico. Journal of Cave and Karst Studies, 62(2), 91-108.

Paris, G., Sessions, A. L., Subhas, A. V., Adkins, J. F., 2013. MC-ICP-MS measurement of $\delta^{34}S$ and $\Delta^{33}S$ in small amounts of dissolved sulfate. Chemical Geology, 345, 50-61.

Paris, G., Adkins, J. F., Sessions, A. L., Webb, S. M., Fischer, W. W., 2014. Neoarchean carbonate–associated sulfate records positive $\Delta^{33}S$ anomalies. Science, 346(6210), 739-741.

Parkhurst, D. L., Appelo, C. A. J., 1999. User's guide to PHREEQC (Version 2): A computer program for speciation, batch-reaction, one-dimensional transport, and inverse geochemical calculations. Water-resources investigations report, 99(4259), 312.

Pérez-Mejías, C., Sancho, C., Gázquez, F., Moreno, A., Bartolome, M., Osácar, M. C., Cheng, H., 2019. Insights into the speleogenesis of Ejulve cave (Iberian Range, NE Spain): quaternary hydrothermal karstification?. Journal of Iberian Geology, 45(3), 511-527.

Piccini, L., 2000. Il carsismo di origine idrotermale del Colle di Monsummano (Pistoia–Toscana). Le Grotte d'Italia V(1): 33-43.

Piccini, L., De Waele, J., Galli, E., Polyak, V. J., Bernasconi, S. M., Asmerom, Y., 2015. Sulphuric acid speleogenesis and landscape evolution: Montecchio cave, Albegna river valley (Southern Tuscany, Italy). Geomorphology, 229, 134-143.

Pin, C., Bassin, C., 1992. Evaluation of a strontium-specific extraction chromatographic method for isotopic analysis in geological materials. Analytica Chimica Acta 269(2), 249-255.

Pin, C., Zalduegui, J. S., 1997. Sequential separation of light rare-earth elements, thorium and uranium by miniaturized extraction chromatography: application to isotopic analyses of silicate rocks. Analytica Chimica Acta, 339(1-2), 79-89.

Plan, L., Tschegg, C., De Waele, J., Spötl, C., 2012. Corrosion morphology and cave wall alteration in an Alpine sulfuric acid cave (Kraushöhle, Austria). Geomorphology, 169, 45-54.

Raab, M., Spiro, B., 1991. Sulfur isotopic variations during seawater evaporation with fractional crystallization. Chemical Geology: Isotope Geoscience section, 86(4), 323-333.

Sansjofre, P., Cartigny, P., Trindade, R. I., Nogueira, A. C., Agrinier, P., & Ader, M. (2016). Multiple sulfur isotope evidence for massive oceanic sulfate depletion in the aftermath of Snowball Earth. Nature communications, 7(1), 1-8.

Sarbu, S. M., Lascu, C., 1997. Condensation corrosion in Movile cave, Romania. Journal of Caves and Karst Studies, 59, 99-102.

Sartégou, A., Blard, P. H., Braucher, R., Bourlès, D., Sorriaux, P., Zimmermann, L., Laffitte, A., Tibari, B., Leanny, L., Guillou, V., Bourdet, A., ASTER Team, 2020. Late Cenozoic evolution of the Ariège River valley (Pyrenees) constrained by cosmogenic 26Al/10Be and 10Be/21Ne dating of cave sediments. Geomorphology, 371.

Séranne, M., 1999. The Gulf of Lion continental margin (NW Mediterranean) revisited by IBS: an overview. Geological Society, London, Special Publications, 156(1), 15-36.

Sibson, R.H., 1992. Fault-valve behavior and the hydrostatic-lithostatic fluid pressure interface. Earth-Sci. Rev. 32, 141-144.

Sim, M. S., Bosak, T., Ono, S., 2011. Large sulfur isotope fractionation does not require disproportionation. Science, 333(6038), 74-77.

Song, H., Wignall, P.B., Tong, J., Song, H., Chen, J., Chu, D., Tian, L., Luo, M., Zong, K., Chen, Y., Lai, X., Zhang, K., Wang, H., 2015. Integrated Sr isotope variations and global environmental changes through the Late Permian to early Late Triassic. Earth Planet Sci. Lett. 424, 140–147.

Sorriaux, P., 1982. Contribution à l'étude de la sédimentation en milieu karstique Le système de Niaux–Lombrives–Sabart (Pyrénées ariégeoises). Doctoral dissertation, Univ Toulouse et Laboratoire Souterrain de Moulis CNRS, 255 p.

Sorriaux, P., Delmas, M., Calvet, M., Gunnell, Y., Durand, N., Edwige, P. B., 2016. Relations entre karst et glaciers depuis 450 ka dans les grottes de Niaux-Lombrives-Sabart (Pyrénées ariégeoises) Nouvelles datations U/Th dans la grotte de Niaux. Karstologia, 67, 3-16.

Taillefer, A., Soliva, R., Guillou-Frottier, L., Le Goff, E., Martin, G., Séranne, M., 2017. Fault-related controls on upward hydrothermal flow: an integrated geological study of the Têt fault system, Eastern Pyrénées (France). Geofluids, 2017.

Temovski, M., Audra, P., Mihevc, A., Spangenberg, J. E., Polyak, V., McIntosh, W., Bigot, J. Y., 2013. Hypogenic origin of Provalata Cave, Republic of Macedonia: a distinct case of successive thermal carbonic and sulfuric acid speleogenesis. International Journal of Speleology, 42(3), 7.

Temovski, M., Futó, I., Túri, M., Palcsu, L., 2018. Sulfur and oxygen isotopes in the gypsum deposits of the Provalata sulfuric acid cave (Macedonia). Geomorphology, 315, 80-90.

Tisato, N., Sauro, F., Bernasconi, S. M., Bruijn, R. H., De Waele, J., 2012. Hypogenic contribution to speleogenesis in a predominant epigenic karst system: a case study from the Venetian Alps, Italy. Geomorphology, 151, 156-163.

Van Stempvoort, D. R., Krouse, H. R., 1994. Controls of $\delta^{18}O$ in sulfate: Review of experimental data and application to specific environments. Environmental Geochemistry of Sulfide Oxidation, 29, 446-480.

Veizer, J., Ala, D., Azmy, K., Bruckschen, P., Buhl, D., Bruhn, F., Carden, G. A. F., Diener, A., Ebneth, S., Godderis, Y., Jasper, T., Korte, C., Pawellek, F., Podlaha, O. G., Strauss, H., 1999. $^{87}Sr/^{86}Sr$, $\delta^{13}C$ and $\delta^{18}O$ evolution of Phanerozoic seawater. Chemical geology, 161(1-3), 59-88.

Worden R. H., Smalley P. C., Oxtoby N. H., 1995. Gas souring by thermochemical sulfate reduction at 140 °C. AAPG Bulletin, 79, 854-863.

Worden, R. H., Smalley, P. C., 1996. H2S-producing reactions in deep carbonate gas reservoirs: Khuff Formation, Abu Dhabi. Chemical Geology, 133(1-4), 157-171.

Wortmann, U. G., Bernasconi, S. M., Böttcher, M. E., 2001. Hypersulfidic deep biosphere indicates extreme sulfur isotope fractionation during single-step microbial sulfate reduction. Geology, 29(7), 647-650.

Zerkle, A. L., Jones, D. S., Farquhar, J., Macalady, J. L., 2016. Sulfur isotope values in the sulfidic Frasassi cave system, central Italy: A case study of a chemolithotrophic S-based ecosystem. Geochimica et Cosmochimica Acta, 173, 373-386.